HAL
open science

On the Time Momentum Representation of Hadronic Vacuum Polarization and $g_\mu - 2$

David Greynat, Eduardo de Rafael

To cite this version:

David Greynat, Eduardo de Rafael. On the Time Momentum Representation of Hadronic Vacuum Polarization and $g_\mu - 2$. Journal of High Energy Physics, 2023, 03, pp.248. 10.1007/JHEP03(2023)248 . hal-03993833

HAL Id: hal-03993833

https://hal.science/hal-03993833v1

Submitted on 12 Sep 2023

HAL is a multi-disciplinary open access archive for the deposit and dissemination of scientific research documents, whether they are published or not. The documents may come from teaching and research institutions in France or abroad, or from public or private research centers.

L'archive ouverte pluridisciplinaire **HAL**, est destinée au dépôt et à la diffusion de documents scientifiques de niveau recherche, publiés ou non, émanant des établissements d'enseignement et de recherche français ou étrangers, des laboratoires publics ou privés.

Published for SISSA by Springer

Received: February 13, 2023
Accepted: March 14, 2023
Published: March 30, 2023

On the time momentum representation of hadronic vacuum polarization and $g_\mu - 2$

David Greynat[a] **and Eduardo de Rafael**[b]

[a] *Grenoble, France*
[b] *Aix-Marseille Univ, Université de Toulon, CNRS, CPT, Marseille, France*

E-mail: david.greynat@gmail.com, EdeR@cpt.univ-mrs.fr

Abstract: We propose a new set of model independent approximants adapted to the time momentum representation (TMR) of hadronic vacuum polarization (HVP) and its contribution to $g_\mu - 2$. They provide a way to extrapolate lattice QCD (LQCD) results obtained in an optimal time-region, to the full range required for an evaluation of the HVP contribution to $g_\mu - 2$. They offer as well a new way to confront LQCD results in restricted TMR regions, with the full contribution obtained from data driven determinations.

Keywords: Algorithms and Theoretical Developments, Electroweak Precision Physics, Specific QCD Phenomenology, Standard Model Parameters

ArXiv ePrint: 2302.01692

Open Access, © The Authors.
Article funded by SCOAP[3].

https://doi.org/10.1007/JHEP03(2023)248

JHEP03(2023)248

Contents

1 Introduction **1**

2 Properties of HVP and its TMR **3**

3 Asymptotic behaviours **5**
3.1 Asymptotic expansions of $G(X)$ and Bessel functions 8
3.2 The skeleton $G^*(X)$ function 9

4 Flajolet-Odlyzko approximants **11**
4.1 The FO-theorem 12
4.2 The FO-approximants in practice 14

5 Illustration with a phenomenological model **16**
5.1 Fits to the model data using FO-approximants 18
5.2 Errors of the FO-approximants 21

6 Conclusion and outlook **23**

A Mathematical details of the FO-theorem **24**

1 Introduction

The measurements of the anomalous magnetic moment of the muon a_μ, made at BNL [1] and more recently at Fermilab [2, 3], give the results:

$$a_\mu^{\rm BNL} = 116\ 592\ 089\ (63) \times 10^{-11} \quad \text{and} \quad a_\mu^{\rm FNAL} = 116\ 592\ 040\ (54) \times 10^{-11}\,. \tag{1.1}$$

They agree with each other at the level of 0.6 standard deviations (0.6σ) and their combined number

$$a_\mu(2021) = 116\ 592\ 040\ (41) \times 10^{-11}\,, \tag{1.2}$$

has the remarkable accuracy of 0.35 parts per million.

The theoretical evaluation of the same observable in the Standard Model has been made to a comparable precision. The result

$$a_\mu(\text{Th. WP}) = 116\ 591\ 810\ (43) \times 10^{-11} \tag{1.3}$$

reported in the 2020 White Paper (WP) of ref. [4] has been the *consensus theory number* for a while. When compared to the experimental number in eq. (1.2) it turns out to be 4.2σ below, a significant difference, which has triggered many speculations on what kind of new physics could explain this difference.

JHEP03(2023)248

The 2020 WP number, however, does not take into account the lattice QCD (LQCD) result of the BMW collaboration [5]

$$a_\mu(\mathrm{HVP})_{\mathrm{BMW}} = 7\ 075\ (55) \times 10^{-11}\,, \tag{1.4}$$

which differs from the evaluations using data-driven dispersion relations [6, 7]:

$$a_\mu(\mathrm{HVP})^{\mathrm{ref.[6]}}_{\mathrm{lowest\ order}} = 6\ 940\ (40) \times 10^{-11} \quad \text{and} \quad a_\mu(\mathrm{HVP})^{\mathrm{ref.[7]}}_{\mathrm{lowest\ order}} = 6\ 928\ (24) \times 10^{-11}\,, \tag{1.5}$$

incorporated in the *consensus theory number* of the 2020 WP. The BMW-lattice QCD result reduces the total discrepancy with the experimental result in eq. (1.2) from 4.2σ to 1.6σ. Still a discrepancy, but not significant to argue evidence for new physics. Recently, the BMW result has also been confirmed, at least partially, by other LQCD collaborations [8–10]. If the disagreement between LQCD and the experimental dispersive evaluations of the HVP persists, one will have to find the explanation for that. The two methods involve integrals of different quantities which makes the comparison difficult but not impossible. A lot of activity on that is underway, mostly concentrated on evaluations of the so called *window observables* proposed in ref. [12] (see e.g. refs. [8, 11, 13] and references therein).

In the meantime, the Fermilab Muon $g-2$ experiment expects to reduce the error of their 2021 result by a factor of four, as more statistics accumulate. There is also a new experiment at the Japan Proton Accelerator Research Complex in Tokai, the J-PARC experiment E34 [14], which will employ a new different technique to measure the muon anomaly. Another expected experiment is the MUonE proposal at the CERN SPS [15–17]. It consists in extracting the value of the HVP self-energy function in the Euclidean from its contribution to the differential cross-section of elastic muon-electron scattering, with muons at $\mathrm{E}_\mu = 160\,\mathrm{GeV}$ colliding on atomic electrons of a fixed low Z target [18]. The muon anomaly can then be obtained from a weighted integral of the measured HVP self-energy function.

The purpose of this paper is to introduce a new type of model independent approximants adapted to the time momentum representation (TMR) of hadronic vacuum polarization used in LQCD evaluations of $a_\mu(\mathrm{HVP})$ at present. The method is based on the *reconstruction approximants* which follow from the *transfer theorem* of Flajolet and Odlyzko [19, 20], and has previously been applied to the MUonE-proposal [21] as well as to other observables (see e.g. refs. [22–24]). We show how to adapt this method to extrapolate the LQCD results obtained in a restricted TMR-interval to the full integration domain required to evaluate $a_\mu(\mathrm{HVP})$.

The paper is organized as follows. Section 2 reviews the properties of HVP and its TMR which will be needed. Section 3 is dedicated to the asymptotic behaviours of the TMR function $G(x_0)$ in QCD, both at short distances and at long distances. As far as we know, some aspects of this section are new, in particular the construction of a skeleton $G^*(x_0)$ function in terms of Bessel functions which provides a first approximant to the TMR $G(x_0)$ function in its full x_0 range. Section 4 discusses the formulation of the reconstruction approximants that follow from the transfer theorem of Flajolet and Odlyzko [19, 20]. The content of this theorem is explained in subsection 4.1, and its

JHEP03(2023)248

application to construct what we call FO-approximants (for short) is discussed in detail in subsection 4.2. Section 5 is dedicated to show how to implement the FO-approximants in practice, and we illustrate this with the example of a phenomenological model which simulates the physical hadronic spectral function. The conclusion and outlook are finally given in section 6. We have relegated to an appendix the mathematical details of the FO-theorem needed in our application.

2 Properties of HVP and its TMR

The function which governs HVP is the Fourier transform of the vacuum expectation value of the time-ordered product of two electromagnetic hadronic currents of the Standard Model $J_\mu^{\rm had}(x)$ at separate space-time x-points:

$$\Pi_{\mu\nu}^{\rm had}(q) = i\int_{-\infty}^{+\infty} d^4x\; e^{iq\cdot x}\langle 0|T\left(J_\mu^{\rm had}(x)J_\nu^{\rm had}(0)\right)|0\rangle = (q_\mu q_\nu - q^2 g_{\mu\nu})\Pi_{\rm had}(q^2)\,. \tag{2.1}$$

The hadronic photon self-energy function $\Pi_{\rm had}(q^2)$ is a complex function of its q^2 variable. It is an analytic function in the full complex plane, but for a cut in the real axis which goes from the physical threshold t_0 to infinity.[1] As such, the on-shell renormalized HVP-function, i.e. $\Pi_{\rm had}(q^2)$ subtracted at its value at $q^2=0$, obeys the dispersion relation:

$$\Pi^{\rm HVP}(q^2) \equiv \Pi_{\rm had}(q^2) - \Pi_{\rm had}(0) = \int_{t_0}^{\infty}\frac{dt}{t}\,\frac{q^2}{t-q^2-i\epsilon}\,\frac{1}{\pi}\,{\rm Im}\,\Pi_{\rm had}(t)\,, \quad t_0 \equiv 4m_{\pi^\pm}^2\,, \tag{2.2}$$

and the optical theorem relates the hadronic spectral function $\frac{1}{\pi}\,{\rm Im}\,\Pi_{\rm had}(t)$ to the one-photon annihilation cross-section into hadrons:

$$\sigma(t)_{e^+e^-\to{\rm had}} \underset{m_e\to 0}{\sim} \frac{4\pi^2\alpha}{t}\,\frac{1}{\pi}\,{\rm Im}\,\Pi_{\rm had}(t)\,. \tag{2.3}$$

The evaluation of the HVP contribution to the anomalous magnetic moment of the muon $a_\mu^{\rm HVP}$ can then be made using the integral representation [25–27]:

$$a_\mu^{\rm HVP} = \frac{\alpha}{\pi}\int_{t_0}^{\infty}\frac{dt}{t}\int_0^1 dx\;\frac{x^2(1-x)}{x^2+\frac{t}{m_\mu^2}(1-x)}\,\frac{1}{\pi}\;{\rm Im}\,\Pi_{\rm had}(t)\,. \tag{2.4}$$

This so called *dispersive method*, is the way that experimental data-driven determinations of $a_\mu^{\rm HVP}$ have been made; the earliest in ref. [27] using the Gounaris-Sakurai parametrization of the pion form factor [28], the latest in refs. [6, 7] using a wealth of experimental results.

A crucial observation made by the authors of ref. [29] is that, in Euclidean space-time and in the special kinematic configuration where $\vec{q}=0$, the $\Pi_{\mu\nu}^{\rm had}(q)$ function in eq. (2.1) becomes

$$\Pi_{ij}^{\rm had}(q_0,\vec{0}) = \int_{-\infty}^{+\infty} dx_0 e^{-iq_0x_0}\underbrace{\int_{-\infty}^{+\infty} d^3\vec{x}\;\delta_{ij}\;\langle 0|T\left(J_i(x_0,\vec{x})J_j(0)\right)|0\rangle}_{G(x_0)}\,, \tag{2.5}$$

[1] In the presence of higher order electromagnetic corrections the threshold is at the mass of the π^0 because of the $\pi^0\gamma$ contribution to the spectral function. In this paper the threshold will be fixed at $t_0 = 4m_{\pi^\pm}^2$, but can be adjusted to $m_{\pi^0}^2$ if necessary.

JHEP03(2023)248

and the underlined time-dependent function $G(x_0)$, for x_0 in an optimal region, is accessible to accurate evaluations in LQCD. The expression of $a_\mu^{\rm HVP}$ in terms of $G(x_0)$, the so called TMR [29], is then given by the integral:

$$a_\mu^{\rm HVP} = \frac{\alpha}{\pi} m_\mu^2 \int_0^\infty dx_0 \, \frac{x_0^4}{2} \, {\rm G}_{3,5}^{2,3}\left((m_\mu x_0)^2 \left| \begin{matrix} -1, -\frac{1}{2}, 0\,; — \\ 0, 1, -3, -\frac{3}{2}, -2 \end{matrix} \right. \right) \\ \times \underbrace{\int_{\sqrt{t_0}}^\infty d\omega \; \omega^2 \; e^{-\omega|x_0|} \frac{1}{\pi} \, {\rm Im}\, \Pi_{\rm had}(\omega^2)}_{G(x_0)} \,, \tag{2.6}$$

where $\omega^2 = t$ (the Minkowski t-variable of the spectral function) and

$$\begin{aligned} &{\rm G}_{3,5}^{2,3}\left((m_\mu x_0)^2 \left| \begin{matrix} -1, -\frac{1}{2}, 0\,; — \\ 0, 1, -3, -\frac{3}{2}, -2 \end{matrix} \right. \right) \\ &\quad = \frac{1}{2\pi i} \int\limits_{c_s - i\infty}^{c_s + i\infty} ds \; (m_\mu x_0)^{-2s} \frac{\Gamma(s)\Gamma(1+s)\Gamma(1-s)\Gamma\left(\frac{3}{2}-s\right)\Gamma(2-s)}{\Gamma(4-s)\Gamma(3-s)\Gamma\left(\frac{5}{2}-s\right)} \,, \end{aligned} \tag{2.7}$$

is a Meijer's G-function.

The TMR-function $G(x_0)$ in eq. (2.6) is the second derivative (with respect to the time variable x_0) of the Laplace transform (with respect to the energy variable ω) of the hadronic spectral function. From the usual definition of the Laplace transform:

$$\mathcal{L}(x_0) = \int_{\sqrt{t_0}}^\infty d\omega \; e^{-wx_0} \; \frac{1}{\pi} \, {\rm Im}\, \Pi_{\rm had}(\omega^2) \,, \tag{2.8}$$

there follows that

$$G(x_0) = \left(-\frac{\partial}{\partial x_0} \right)^2 \mathcal{L}(x_0) = \int_{\sqrt{t_0}}^\infty d\omega \; e^{-\omega x_0} \; \omega^2 \frac{1}{\pi} \, {\rm Im}\, \Pi_{\rm had}(\omega^2) \,. \tag{2.9}$$

Because of the positivity of the hadronic spectral function, both functions $\mathcal{L}(x_0)$ and $G(x_0)$ as well as the successive derivatives $\left(-\frac{\partial}{\partial x_0}\right)^p G(x_0)$, $p = 1, 2, 3, \ldots$, are all monotonously decreasing functions of x_0 for $0 \le x_0 \le \infty$; a well known property as well of the Mellin transform of the hadronic spectral function [30]

$$\mathcal{M}(s) = \int_{t_0}^\infty \frac{dt}{t} \left(\frac{t}{t_0} \right)^{s-1} \frac{1}{\pi} \, {\rm Im}\, \Pi_{\rm had}(t) \,, \tag{2.10}$$

as a function of ${\rm Re}(s) < 1$.

An alternative way to evaluate $a_\mu^{\rm HVP}$ to the one in eq. (2.6), is to use the integral representation

$$\Pi^{\rm HVP}(-Q^2) = 2 \int_0^\infty dx_0 \; \left[1 - \cos\left(\sqrt{Q^2} x_0 \right) \right] \; \mathcal{L}(x_0) \,, \tag{2.11}$$

equivalent to [29]

$$\Pi^{\rm HVP}(-Q^2) = 2 \int_0^\infty dx_0 \left[\frac{1 - \cos\left(\sqrt{Q^2} x_0 \right)}{Q^2} - \frac{x_0^2}{2} \right] \; G(x_0) \,, \tag{2.12}$$

JHEP03(2023)248

and then the Euclidean representation of the anomaly proposed in refs. [31–33]:

$$a_\mu^{\rm HVP} = -\frac{\alpha}{\pi}\int_0^1 dx\ (1-x)\ \Pi^{\rm HVP}\left(-\frac{x^2}{1-x}m_\mu^2\right)\,, \quad Q^2 \equiv \frac{x^2}{1-x}m_\mu^2\,. \tag{2.13}$$

3 Asymptotic behaviours

The TMR-function $G(x_0)$ has a Mellin-Barnes representation which can be obtained by inserting the identity

$$e^{-\omega x_0} = \frac{1}{2\pi i}\int\limits_{c_s-i\infty}^{c_s+i\infty} ds\ (\omega x_0)^{-s}\ \Gamma(s)\,, \quad c_s \equiv {\rm Re}(s) > 0\,, \tag{3.1}$$

in the integrand of eq. (2.9) (recall that $t=\omega^2$) and following the steps:

$$G(x_0) = \int_{\sqrt{t_0}}^\infty d\omega\ e^{-\omega x_0}\ \omega^2\ \frac{1}{\pi}\,{\rm Im}\,\Pi_{\rm had}(\omega^2) \tag{3.2}$$

$$= \frac{1}{2\pi i}\int\limits_{c_s-i\infty}^{c_s+i\infty} ds\ x_0^{-s}\ \Gamma(s)\frac{1}{2}\int_{t_0}^\infty \frac{dt}{t}\ t^{3/2-s/2}\frac{1}{\pi}\,{\rm Im}\,\Pi_{\rm had}(t) \qquad (t\equiv\omega^2)$$

$$= \frac{t_0^{3/2}}{2}\frac{1}{2\pi i}\int\limits_{c_s-i\infty}^{c_s+i\infty} ds\ \left(x_0\sqrt{t_0}\right)^{-s}\ \ \Gamma(s)\ \mathcal{M}(5/2-s/2)\,, \qquad c_s \equiv {\rm Re}(s) > 3$$

$$= t_0^{3/2}\ \frac{1}{X^5}\ \frac{1}{2\pi i}\int\limits_{c_s-i\infty}^{c_s+i\infty} ds\left(\frac{1}{X^2}\right)^{-s}\Gamma(5-2s)\ \mathcal{M}(s)\,, \qquad c_s \equiv {\rm Re}(s) < 1\,, \tag{3.3}$$

where going from the second line to the third we have used the definition of the Mellin transform of the spectral function in eq. (2.10), and from the third line to the fourth we have introduced the dimensionless variable

$$X \doteq x_0\sqrt{t_0}\,, \tag{3.4}$$

and redefined the integration s-variable. From here onwards we shall often work with the dimensionless TMR-$G(X)$ function:

$$G(X) \equiv \int_1^\infty d\hat\omega\ e^{-\hat\omega X}\hat\omega^2\frac{1}{\pi}\,{\rm Im}\,\Pi_{\rm had}(\hat\omega^2 t_0) = \frac{1}{t_0^{3/2}}G(x_0)\,, \tag{3.5}$$

where

$$\hat\omega \equiv \frac{\omega}{\sqrt{t_0}}\,. \tag{3.6}$$

The TMR of the muon anomaly with this redefinition in terms of the dimensionless variable X is then:

$$a_\mu^{\rm HVP} = \frac{\alpha}{\pi}\frac{m_\mu^2}{t_0}\int_0^\infty dX\ \mathcal{K}(X)\ X^3\ G(X)\,, \tag{3.7}$$

JHEP03(2023)248

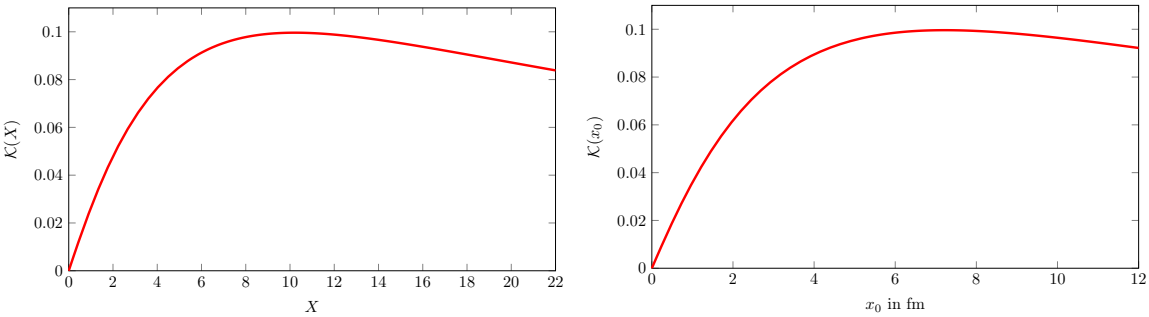

Figure 1. Plots of the kernel $\mathcal{K}(X)$ in eq. (3.8) versus X and versus x_0 in Fermi units.

with

$$\mathcal{K}(X) = \frac{X}{2}\, \mathrm{G}^{2,3}_{3,5}\left(\frac{m_\mu^2}{t_0}\, X^2 \,\middle|\, \begin{matrix} -1, -\frac{1}{2}, 0\,; \,— \\ 0, 1, -3, -\frac{3}{2}, -2 \end{matrix}\right) \tag{3.8}$$

the integration kernel. Figure 1 shows the familiar shape of this kernel, as a function of X and as a function of x_0 in Fermi units for comparison.

The Mellin-Barnes representation of $G(X)$ that follows from eq. (3.3) is:

$$G(X) = \frac{1}{X^5}\, \frac{1}{2\pi i} \int\limits_{c_s - i\infty}^{c_s + i\infty} ds \left(\frac{1}{X^2}\right)^{-s} \Gamma(5-2s)\, \mathcal{M}(s)\,, \quad c_s \equiv \mathrm{Re}(s) < 1\,, \tag{3.9}$$

where the QCD dynamics is fully encoded in the Mellin transform of the hadronic spectral function $\mathcal{M}(s)$ defined in eq. (2.10). The *singular expansion* [34] of the s-integrand in this representation produces the following series expansion for $0 \leq X \leq 1$ (i.e. *short distances*):

$$G(X) \underset{X\to 0}{\sim} \frac{\alpha}{\pi} \left\{ \frac{a_{-3}}{X^3} + \frac{a_{-1}}{X} + \sum_{n=1}^{\infty} \left[a_n + b_n \log X\right] X^n \right\}. \tag{3.10}$$

The coefficient a_{-3} of the leading term is fixed by the residue of the QCD Mellin transform at $s = 1$ which, to leading order in pQCD, is

$$a_{-3} = \frac{N_c}{3} \sum_{\text{quarks}} e_q^2 \times 2\,. \tag{3.11}$$

The next coefficient a_{-1} is governed by the quark mass terms of $\mathcal{O}\left(1/Q^2\right)$ in the expansion of $\Pi_{\text{had}}(-Q^2)$ at large Q^2. The contribution from the light quark masses to a_{-1} vanishes in the chiral limit. The form of the rest of the asymptotic series in eq. (3.10) assumes that the singularities at $s = 1, 2, 3, \cdots$ of $\mathcal{M}(s)$ are simple poles, otherwise higher power $\log X$-terms must also be included. Let us recall (see e.g. ref. [21]) that the singularities of $\mathcal{M}(s)$ at $s = 1, 2, 3, \ldots$ govern the asymptotic expansion of the hadronic self-energy at large Q^2. The coefficients a_n and b_n, however, will become free parameters in our approach; only the value of a_{-3} in eq. (3.11) will be used as an input.

The Mellin-Barnes representation in eq. (3.9) does not give, however, direct information about the behaviour of $G(X)$ at large-X (i.e. *long-distances*). This is because the *fundamental strip* [34] where the integral in eq. (3.9) converges goes all the way from

JHEP03(2023)248

$\mathrm{Re}(s) < 1$ to $\mathrm{Re}(s) = -\infty$. One can nevertheless show, using inverse Laplace-transform properties [35], that the large-X behaviour of $G(X)$ is related to the $\hat{\omega} \to 1$ threshold behaviour of the hadronic spectral function, i.e. to the power series:

$$\hat{\omega}^2 \, \frac{1}{\pi} \, \mathrm{Im}\, \Pi_{\mathrm{had}}(\hat{\omega}^2 t_0) \underset{\hat{\omega}\to 1}{\sim} \frac{\alpha}{\pi} \, (\hat{\omega}-1)^{3/2} \sum_{n=0}^{\infty} \chi_n (\hat{\omega}-1)^n \,, \tag{3.12}$$

where, to lowest order in chiral perturbation theory (χPT)

$$\chi_0 \Rightarrow \frac{1}{3\sqrt{2}} \,, \quad \chi_1 \Rightarrow \frac{-1}{12\sqrt{2}} \,, \quad \chi_2 \Rightarrow \frac{11}{96\sqrt{2}} \,, \quad \cdots \,. \tag{3.13}$$

Higher order χPT corrects these values by a series in threshold t_0-powers:

$$\chi_0 \Rightarrow \frac{1}{3\sqrt{2}} \left(1 + \frac{1}{3} \langle \mathrm{r}^2 \rangle_{\pi^\pm} \, t_0 + \cdots \right) \,, \quad \chi_1 \Rightarrow \frac{-1}{12\sqrt{2}} \left(1 - \frac{7}{3} \langle \mathrm{r}^2 \rangle_{\pi^\pm} \, t_0 + \cdots \right) \quad \cdots \,, \tag{3.14}$$

where e.g., at the one loop level in χPT [36]

$$\langle \mathrm{r}^2 \rangle_{\pi^\pm} = \frac{12 \mathrm{L}_9(\mu)}{f_\pi^2} - \frac{1}{32\pi^2 f_\pi^2} \left[2 \log \left(\frac{m_\pi^2}{\mu^2} \right) + \log \left(\frac{m_K^2}{\mu^2} \right) + 3 \right] \,, \tag{3.15}$$

and the low-energy constant $\mathrm{L}_9(\mu)$ can be obtained, either from experiment [37]:

$$\langle \mathrm{r}^2 \rangle_{\pi^\pm} = (0.439 \pm 0.008)\, \mathrm{fm}^2 \quad \Rightarrow \quad \mathrm{L}_9(M_\rho) = (6.9 \pm 0.7) \times 10^{-3} \,, \tag{3.16}$$

or from LQCD determinations which are in good agreement (see e.g. ref. [38]) with the experimental value.

Numerically

$$\chi_0 = \frac{1}{3\sqrt{2}} \left(1 + \frac{1}{3} \langle \mathrm{r}^2 \rangle_{\pi^\pm} \, t_0 \right) = 0.284 \pm 0.001 \,, \tag{3.17}$$

and

$$\chi_1 = \frac{-1}{12\sqrt{2}} \left(1 - \frac{7}{3} \langle \mathrm{r}^2 \rangle_{\pi^\pm} \, t_0 \right) = 0.026 \pm 0.002 \,. \tag{3.18}$$

Inserting the threshold expansion in the integrand of the $G(X)$ function in eq. (3.5) leads to the *long-distance* behaviour of $G(X)$ in terms of a series of simple Laplace transforms:

$$G(X) \underset{X\to\infty}{\sim} \frac{\alpha}{\pi} \sum_{n=0}^{\infty} \chi_n \, e^{-X} \int_1^\infty d\hat{\omega} \, e^{-(\hat{\omega}-1)X} (\hat{\omega}-1)^{n+3/2} \tag{3.19}$$

$$= \frac{\alpha}{\pi} \frac{e^{-X}}{X^{\frac{5}{2}}} \sum_{n=0}^{\infty} \chi_n \, \Gamma\left(\frac{5}{2} + n \right) \frac{1}{X^n} \,. \tag{3.20}$$

This series, however, is a divergent series (though Borel summable in all the models we have examined), which implies that both the small-X expansion as well as the large-X expansion of $G(X)$ will participate in the application of the transfer theorem of Flajolet and Odlyzko [19, 20] that we shall later discuss.

JHEP03(2023)248

3.1 Asymptotic expansions of $G(X)$ and Bessel functions

An interesting observation about the *long distance* behaviour of $G(X)$ in eq. (3.19) is that each term of the series in the r.h.s. can be expressed as a sum of modified Bessel functions of the second kind $\mathrm{K}_n(X)$ (`BesselK[n,X]` in Wolfram's Mathematica notation). This follows from the integral representation:[2]

$$\mathrm{K}_n(X) = \frac{2^{-n}\sqrt{\pi}}{\Gamma(n+1/2)} X^n \int_1^\infty d\hat{\omega}\; e^{-X\hat{\omega}} (\hat{\omega}^2-1)^{n-1/2}\,, \tag{3.21}$$

and the fact that the series expansion in eq. (3.12) can be rearranged as follows:

$$\hat{\omega}^2\, \frac{1}{\pi}\, \mathrm{Im}\, \Pi_{\mathrm{had}}(\hat{\omega}^2 t_0) \underset{\hat{\omega}\to 1}{\sim} \frac{\alpha}{\pi}\, (\hat{\omega}^2-1)^{3/2} \sum_{n=0}^{\infty} \hat{\chi}_n (\hat{\omega}^2-1)^n\,, \tag{3.22}$$

with the coefficients $\hat{\chi}_n$ recursively related to the χ_n-coefficients in eq. (3.20):

$$\begin{aligned} &\chi_0 = 2\sqrt{2}\hat{\chi}_0\,, \quad \chi_1 = \frac{11}{\sqrt{2}}\hat{\chi}_0 + 4\sqrt{2}\hat{\chi}_1\,, \\ &\chi_2 = \left(\frac{3}{8\sqrt{2}} + 5\sqrt{2}\right)\hat{\chi}_1 + 13\sqrt{2}\hat{\chi}_2 + 8\sqrt{2}\hat{\chi}_3\,, \quad \cdots \end{aligned} \tag{3.23}$$

The equivalent *long-distance* asymptotic behaviour of $G(X)$ in terms of the $\hat{\chi}_n$-series in eq. (3.22) is then

$$G(X) \underset{X\to\infty}{\sim} \frac{\alpha}{\pi} \sum_{n=0}^{\infty} \hat{\chi}_n\, e^{-X} \frac{\partial^2}{\partial X^2} \left(\int_1^\infty d\hat{\omega}\; e^{-X\hat{\omega}} (\hat{\omega}^2-1)^{n+3/2} \right) \tag{3.24}$$

which, using the integral representation of the Bessel function in eq. (3.21), becomes

$$G(X) \underset{X\to\infty}{\sim} \frac{\alpha}{\pi} \sum_{n=0}^{\infty} \hat{\chi}_n\, e^{-X}\, \frac{2^{n+2}\Gamma(n+5/2)}{\sqrt{\pi}}\, \frac{\partial^2}{\partial X^2} \left[\frac{1}{X^{n+2}} \mathrm{K}_{n+2}(X) \right]\,, \tag{3.25}$$

and

$$\begin{aligned} \frac{\partial^2}{\partial X^2} \left[\frac{1}{X^{n+2}} \mathrm{K}_{n+2}(X) \right] &= \frac{1}{X^{5+n}} [(20+18n+4n^2)X + X^3] \mathrm{K}_n(X) \\ &\quad + \frac{1}{X^{5+n}} [40+76n+44n^2+8n^3+(7+4n)X^2]\; \mathrm{K}_{n+1}(X)\,. \end{aligned} \tag{3.26}$$

In particular, the $n=0$ term of the series in eq. (3.25) is

$$3\hat{\chi}_0\, \frac{e^{-X}}{X^5} \left[(20X+X^3)\mathrm{K}_0(X) + (40+7X^2)\mathrm{K}_1(X) \right] \tag{3.27}$$

which, using the fact that

$$\mathrm{K}_n(X) \underset{X\to\infty}{\sim} e^{-X} \sqrt{\frac{\pi}{2}} \left(\frac{1}{X^{1/2}} + \frac{4n^2-1}{8} \frac{1}{X^{3/2}} + \cdots \right)\,, \tag{3.28}$$

[2] See e.g. ref. [39].

JHEP03(2023)248

reproduces the leading behaviour of $G(X)$ at $X \to \infty$ in eq. (3.20) because:

$$3\hat{\chi}_0 \, \frac{e^{-X}}{X^5} \left[(20X + X^3)\mathrm{K}_0(X) + (40 + 7X^2)\mathrm{K}_1(X) \right] \underset{X\to\infty}{\sim} 3\hat{\chi}_0 \sqrt{\frac{\pi}{2}} \, \frac{e^{-X}}{X^{5/2}} \, . \tag{3.29}$$

Another observation about Bessel functions concerns the asymptotic behaviour of $G(X)$ at small-X. It is the fact that $\mathrm{K}_0(X) \underset{X\to 0}{=} \mathcal{O}(\ln X)$ and $\mathrm{K}_\nu(X) \underset{X\to 0}{=} \mathcal{O}(X^{-\nu})$ for $\nu \neq 0$ and in particular

$$\mathrm{K}_3(X) \underset{X\to 0}{\sim} \frac{8}{X^3} - \frac{1}{X} + \frac{X}{8} + \frac{X^3}{576}(12 \log X - 11 + 12\gamma_{\mathrm{E}} - 12 \log 2) + \cdots \, , \tag{3.30}$$

which has the same $\mathcal{O}(X^{-3})$ leading behaviour as $G(X)$ in QCD at $X \to 0$.

These observations about Bessel functions suggest considering the minimal linear combination of $\mathrm{K}_n(X)$-functions, modulated by X-polynomials, which reproduces the leading asymptotic behaviours of $G(X)$ in QCD, both at short distances and at long-distances. We call this the *skeleton* $G^*(X)$ *approximant* of the physical $G(X)$ and discuss its construction in the next subsection.

3.2 The skeleton $G^*(X)$ function

The function in question must be of the form:

$$G^*(X) = \frac{\alpha}{\pi} \left[a_{-3} \frac{1}{8} \mathrm{K}_3(X) + (A_{1,0} + A_{1,1}X)\, \mathrm{K}_1(X) + (A_{0,0} + A_{0,1}X)\, \mathrm{K}_0(X) \right] , \tag{3.31}$$

with a_{-3} the same coefficient as in eq. (3.11), and the coefficients $A_{i,j}$ adjusted so as to reproduce the leading threshold behaviour of $G(X)$ in eq. (3.20). This requires a set of constraints on the $A_{i,j}$ coefficients so that

$$G^*(X) \underset{X\to\infty}{\sim} \frac{\alpha}{\pi} \, \frac{3}{4} \sqrt{\pi} \, \chi_0 \, \frac{e^{-X}}{X^{5/2}} \, . \tag{3.32}$$

The constraints follow from the fact that the $G^*(X)$ function in eq. (3.31) has the asymptotic expansion:

$$\begin{aligned} \frac{\pi}{\alpha} \sqrt{\frac{2}{\pi}} \, e^X G^*(X) \underset{X\to\infty}{=} & \, [A_{0,0} + A_{1,1}] \sqrt{X} \\ & + \frac{1}{8} \left[a_{-3} + 8A_{0,0} - A_{0,1} + 8A_{1,0} + 3A_{1,1} \right] \frac{1}{\sqrt{X}} \\ & + \frac{1}{128} \left[70a_{-3} - 16A_{0,0} + 9A_{0,1} + 48A_{1,0} - 15A_{1,1} \right] \frac{1}{X^{\frac{3}{2}}} \\ & + \frac{3}{1024} \left[315a_{-3} + 24A_{0,0} - 5\,(5A_{0,1} + 8A_{1,0} - 7A_{1,1}) \right] \frac{1}{X^{\frac{5}{2}}} \\ & + \mathcal{O}\left[\frac{1}{X^{\frac{7}{2}}} \right] , \end{aligned} \tag{3.33}$$

which, in order to agree with the leading behaviour in eq. (3.32), forces the coefficients of the first three terms of this expansion to vanish and the coefficient of the fourth term to

JHEP03(2023)248

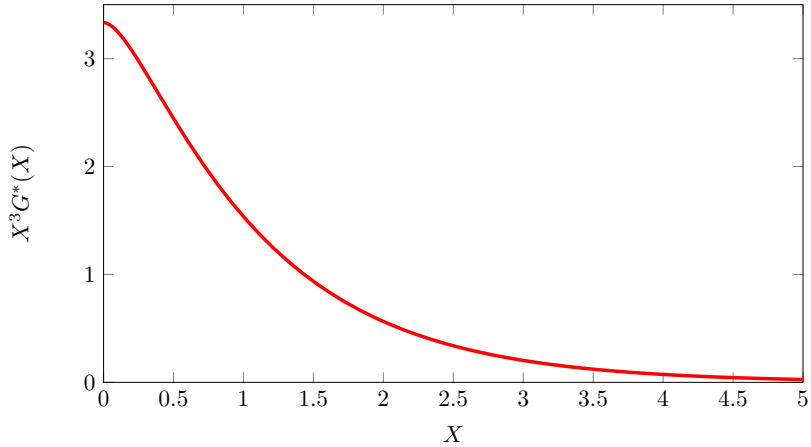

Figure 2. Plot in $\frac{\alpha}{\pi}$ units of the *skeleton function* $X^3\ G^*(X)$ in eq. (3.34) versus X.

reproduce the result in eq. (3.32). The solution of this system of four linear equations with four unknowns is unique and the $G^*(X)$ function is then completely determined in terms of the two parameters a_{-3} and χ_0 with the result

$$\begin{aligned} G^*(X) = \frac{\alpha}{\pi} \Bigg\{ & \frac{a_{-3}}{8}\ \mathrm{K}_3(X) \\ & + \left[-\frac{33}{8}\ a_{-3} + 2\sqrt{2}\ \chi_0 - \left(12\ a_{-3} - 8\sqrt{2}\ \chi_0\right) X \right] \mathrm{K}_1(X) \\ & + \left[10\ a_{-3} - 6\sqrt{2}\ \chi_0 + \left(12\ a_{-3} - 8\sqrt{2}\ \chi_0\right) X \right] \mathrm{K}_0(X) \Bigg\}\ . \end{aligned} \tag{3.34}$$

The shape of the function $X^3\ G^*(X)$ (in $\frac{\alpha}{\pi}$ units), for $a_{-3} = 10/3$ and the central value $\chi_0 = 0.28$ in eq. (3.17), is shown in figure 2. As expected, it is a monotonic decreasing function. A quality test of the *skeleton interpolating approximant* $G^*(X)$ is its contribution to the muon anomaly. The result ($\mathcal{K}(X)$ is the same kernel as in eq. (3.8))

$$a_\mu^{\mathrm{HVP}}[G^*] = \frac{\alpha}{\pi} \frac{m_\mu^2}{t_0} \int_0^\infty dX\ \mathcal{K}(X)\ X^3 G^*(X) = 7\ 533 \times 10^{-11} \tag{3.35}$$

reproduces the central value of, e.g. the LQCD determination in eq. (1.4), at the 6% level, not bad for a first approximation to the physical $G(X)$.

We have also evaluated analytically the associated spectral function to $G^*(X)$, i.e. the *skeleton spectral function* $\frac{1}{\pi}\,\mathrm{Im}\,\Pi^*(t)$ such that

$$G^*(X) = \int_1^\infty d\hat{\omega}\ e^{-\hat{\omega} X} \hat{\omega}^2 \frac{1}{\pi}\,\mathrm{Im}\,\Pi^*(\hat{\omega}^2 t_0)\,. \tag{3.36}$$

The derivation follows from the analytic properties of the Bessel functions which define $G^*(X)$ with the result

$$\frac{1}{\pi}\,\mathrm{Im}\,\Pi^*(t = \hat{\omega}^2 t_0) = \frac{\alpha}{\pi}\ \frac{(\hat{\omega}-1)^2\ \left[a_{-3}\,(\hat{\omega}-1)\ (\hat{\omega}+4) + 4\sqrt{2}\ \chi_0\right]}{2\ \hat{\omega}^2\ (1+\hat{\omega})\ \sqrt{\hat{\omega}^2-1}}\,. \tag{3.37}$$

JHEP03(2023)248

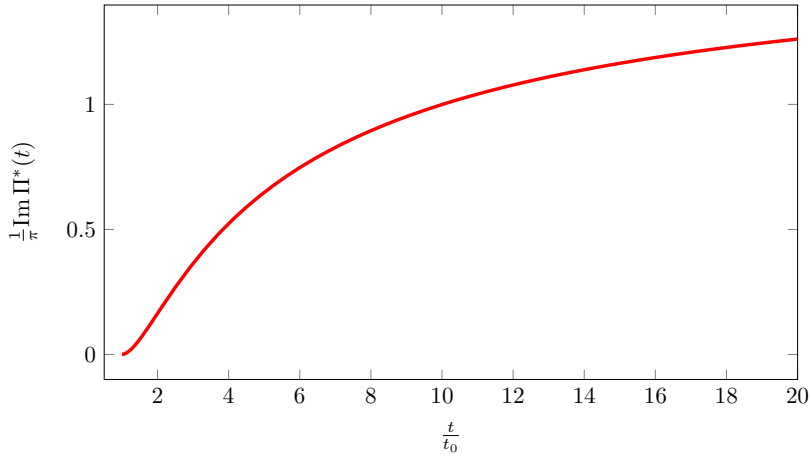

Figure 3. Plot in $\frac{\alpha}{\pi}$ units of the *skeleton spectral function* $\frac{1}{\pi}\,\mathrm{Im}\,\Pi^*(t)$ in eq. (3.37) versus $\frac{t}{t_0}$.

The shape of this spectral function plotted in figure 3 (in $\frac{\alpha}{\pi}$ units) shows a smooth interpolation of the two asymptotic leading behaviours of the HVP spectral function:

$$\begin{aligned}
&\frac{1}{\pi}\,\mathrm{Im}\,\Pi^*(t=\hat{\omega}^2 t_0) \underset{\hat{\omega}\,\to 1}{\sim} \frac{\alpha}{\pi}\,\frac{1}{12}(\hat{\omega}-1)^{\frac{3}{2}}\left(1+\frac{1}{3}\langle \mathrm{r}^2\rangle_{\pi^\pm}\,t_0\right)\,,\\
&\frac{1}{\pi}\,\mathrm{Im}\,\Pi^*(t=\hat{\omega}^2 t_0) \underset{\hat{\omega}\to\infty}{\sim} \frac{\alpha}{\pi}\,\frac{5}{3}\,.
\end{aligned} \tag{3.38}$$

Our choice of a *skeleton function* is of course not unique. Any monotonically decreasing function that interpolates the leading asymptotic behaviours of $G(X)$ at long and short distances in QCD is a possible choice. One may even choose as a *skeleton* $G^*(X)$ *function* the one provided by the data-driven determination of the HVP spectral function, as suggested in the Outlook. Our choice, however, is good enough to implement the approximants that we discuss in the next section. These approximants do not depend on the choice of the *skeleton function*, only the speed of their convergence depends.

4 Flajolet-Odlyzko approximants

We next discuss how to improve on the *skeleton approximant* $G^*(X)$ that we have chosen. The function

$$G_{\mathrm{FO}}(X) \equiv \frac{G(X)}{G^*(X)} - 1 \tag{4.1}$$

defines the deviation of the hadronic $G(X)$ function that we want to reconstruct from the chosen skeleton $G^*(X)$ function. The reason why we introduce this $G_{\mathrm{FO}}(X)$ function is that it no longer has an exponential behaviour at long-distances and, therefore, it is better adapted to an application of the transfer theorem of Flajolet and Odlyzko [19] (FO-theorem for short, hence the subscript FO in $G_{\mathrm{FO}}(X)$). Given some values of $G(X)$ in a finite X region (i.e. a finite x_0 region), we shall first apply the FO-theorem to reconstruct the corresponding $G_{\mathrm{FO}}(X)$ function in its full x_0 range and then, from this reconstruction, the one of the $G(X)$ function will follow from eq. (4.1).

JHEP03(2023)248

The asymptotic expansions of $G_{\rm FO}(X)$ can be deduced from the fact that we know $G^*(X)$ explicitly, as well as the parametrizations of the expansions at small-X and large-X of $G(X)$, with the results

$$G_{\rm FO}(X) \underset{X\to 0}{\sim} \sum_{\ell\geqslant 0, n\geqslant 2+\ell} \mathrm{s}_{n,\ell}\, X^n \ln^\ell X \qquad \text{and} \qquad G_{\rm FO}(X) \underset{X\to\infty}{\sim} \sum_{n\geqslant 1} \frac{\mathrm{l}_n}{X^n}\,. \tag{4.2}$$

where e.g.

$$\mathrm{s}_{2,0} = \frac{a_{-1} - 2\sqrt{2}\chi_0}{a_{-3}} + \frac{17}{4}\,, \tag{4.3}$$

$$\mathrm{s}_{3,0} = \frac{a_0 + 2a_{-3}(6 + 5\gamma_E - 5\ln 2) + 2\sqrt{2}\chi_0(-4 - 3\gamma_E + \ln 8)}{a_{-3}}\,, \tag{4.4}$$

$$\mathrm{s}_{3,1} = 10 - \frac{6\sqrt{2}\chi_0}{a_{-3}}\,, \tag{4.5}$$

$$\cdots$$

$$\mathrm{l}_1 = \frac{5\left(-5\sqrt{2}a_{-3} + 6\chi_0 + 8\chi_1\right)}{16\chi_0}\,, \tag{4.6}$$

$$\mathrm{l}_2 = \frac{5}{128}\frac{-5\sqrt{2}a_{-3}\left(73\chi_0 + 100\chi_1\right) + 625a_{-3}^2 + 5\chi_0\left(-15\chi_0 + 120\chi_1 + 224\chi_2\right)}{128\chi_0^2}\,, \tag{4.7}$$

$$\cdots$$

4.1 The FO-theorem

This theorem relates the non-analyticity of a function defined in a finite domain, to the large order behaviour of the coefficients of its Taylor expansion at values where it is analytic.

In order to apply this theorem in our case we first project the domain $0 \leq X \leq \infty$ to a finite one using the mapping:

$$X \mapsto \varphi = \frac{1 - X^2}{1 + X^2} \Longleftrightarrow X \mapsto \frac{\sqrt{1-\varphi}}{\sqrt{1+\varphi}} \Longleftrightarrow \begin{cases} X \to 0 \Longleftrightarrow \varphi \to 1 \\ X \to 1 \Longleftrightarrow \varphi \to 0 \\ X \to \infty \Longleftrightarrow \varphi \to -1 \end{cases} \tag{4.8}$$

that projects X to the domain $|\varphi| \leqslant 1$. The FO-theorem is then encoded in the identity:

$$G_{\rm FO}\left(X = \frac{\sqrt{1-\varphi}}{\sqrt{1+\varphi}}\right) = \sum_{n=0}^{\infty} \underbrace{\left(g_n - g_n^{\rm AS}\right)}_{\mathcal{A}_n} \varphi^n + \underbrace{\sum_{n=1}^{\infty} g_n^{\rm AS}\, \varphi^n}_{G_{\rm FO}^{\rm sing}(\varphi)}\,, \tag{4.9}$$

where the g_n denote the coefficients of the Taylor expansion of $G_{\rm FO}(X)$ at $\varphi \to 0$ and the $g_n^{\rm AS}$ the coefficients of the same Taylor series as $n \to \infty$. The FO-theorem relates the $g_n^{\rm AS}$ coefficients to the non-analyticity of the $G_{\rm FO}(X)$ function at short distances ($\varphi \to 1$) and at long-distances ($\varphi \to -1$). The second term in the r.h.s. of eq. (4.9) denotes the singular function $G_{\rm FO}^{\rm sing}(\varphi)$ that emerges from the sums of the asymptotic power series at $\varphi \to 1$ and at $\varphi \to -1$.

JHEP03(2023)248

More precisely, the Taylor expansion of the $G_{\rm FO}$ function at $X \to 1$ becomes now a Taylor expansion at $\varphi \to 0$:

$$G_{\rm FO}\left(X = \frac{\sqrt{1-\varphi}}{\sqrt{1+\varphi}}\right) \underset{\varphi\to 0}{\sim} \sum_{n=0}^{\infty} g_n \varphi^n \,. \tag{4.10}$$

Then:

- At short distances $\varphi \to 1$, and from the expansion at $X \to 0$ in eq. (4.2), one gets:

$$G_{\rm FO}\left(\frac{\sqrt{1-\varphi}}{\sqrt{1+\varphi}}\right) \underset{\varphi\to 1}{\sim} \frac{\mathrm{s}_{2,0}}{2}(1-\varphi) + \frac{2\,\mathrm{s}_{3,0} - \ln 2\,\mathrm{s}_{3,1}}{4\sqrt{2}}(1-\varphi)^{\frac{3}{2}} + \frac{\mathrm{s}_{3,1}}{4\sqrt{2}}(1-\varphi)^{\frac{3}{2}}\ln(1-\varphi) + \cdots \,. \tag{4.11}$$

  The second and third terms in this series are at the origin of the leading non-analytic contributions when $\varphi \to 1$. The FO-theorem relates them to the n-behaviour of their contribution to the $g_n^{\rm AS}$ coefficients in eq. (4.9) as follows (see the appendix for details):

$$(1-\varphi)^{\frac{3}{2}} \longmapsto \frac{2}{\sqrt{\pi}}\frac{1}{n^{\frac{5}{2}}}\left[1 + \frac{15}{8}\frac{1}{n} + \frac{385}{128}\frac{1}{n^2} + \cdots\right] , \tag{4.12}$$

  and

$$(1-\varphi)^{\frac{3}{2}}\ln(1-\varphi) \longmapsto \frac{2}{\sqrt{\pi}}\frac{1}{n^{\frac{5}{2}}}\left\{\frac{8}{3} - \gamma_E - \ln 4 - \ln n + \frac{15}{8}\left[\frac{56}{15} - \gamma_E - \ln 4 - \ln n\right]\frac{1}{n} + \cdots\right\} . \tag{4.13}$$

  The leading terms of these two asymptotic behaviours i.e., the term proportional to $\frac{1}{n^{5/2}}$ in eq. (4.12) and the term proportional to $\frac{1}{n^{5/2}}\log n$ in eq. (4.13), generate then the following singular functions:

$$\sum_{n=1}^{\infty}\frac{\varphi^n}{n^{5/2}} = \mathrm{Li}_{5/2}(\varphi) \quad \text{and} \quad -\sum_{n=1}^{\infty}\frac{\log n}{n^{5/2}}\varphi^n = \mathrm{Li}_{5/2}^{(1,0)}(\varphi) \,, \tag{4.14}$$

  where

$$\mathrm{Li}_a^{(1,0)}(x) \doteq \frac{d}{ds}\mathrm{Li}_s(x)\Big|_{s=a} . \tag{4.15}$$

  These singular functions, modulated by their corresponding coefficients, are then to be included in the function $G_{\rm FO}^{\rm sing}(\varphi)$ in eq. (4.9).

- At long distances $\varphi \to -1$, and from the expansion at $X \to \infty$ in eq. (4.2), one gets:

$$G_{\rm FO}\left(X = \frac{\sqrt{1-\varphi}}{\sqrt{1+\varphi}}\right) \underset{\varphi\to -1}{\sim} \frac{\mathrm{l}_1}{\sqrt{2}}\sqrt{1+\varphi} + \frac{\mathrm{l}_2}{2}(1+\varphi) + \frac{\mathrm{l}_1 - 2\,\mathrm{l}_3}{4\sqrt{2}}(1+\varphi)^{\frac{3}{2}} + \cdots \,. \tag{4.16}$$

  The first term in the r.h.s. is at the origin of the leading non-analytic contribution when $\varphi \to -1$. The FO-theorem relates it to the n-behaviour of its contribution to the $g_n^{\rm AS}$ coefficients in eq. (4.9) as follows (see the appendix for details):

$$\sqrt{1+\varphi} \longmapsto -\frac{(-1)^n}{2\sqrt{\pi}}\frac{1}{n^{\frac{3}{2}}}\left[1 + \frac{3}{8}\frac{1}{n} + \frac{25}{128}\frac{1}{n^2} + \cdots\right] . \tag{4.17}$$

JHEP03(2023)248

The leading term proportional to $\frac{1}{n^{3/2}}$ generates then the singular function

$$\sum_{n=1}^{\infty} \frac{(-1)^n \varphi^n}{n^{3/2}} = \mathrm{Li}_{3/2}(-\varphi) \tag{4.18}$$

that modulated by its corresponding coefficient, contributes to $G_{\mathrm{FO}}^{\mathrm{sing}}(\varphi)$ in eq. (4.9).

4.2 The FO-approximants in practice

A priori, the problem to implement in QCD the procedure discussed above is that, except for the coefficients a_{-3} and χ_0, the other coefficients of the asymptotic expansions are not known from first principles and, therefore, practically all the coefficients $\mathrm{s}_{n,l}$ and l_n in eqs. (4.2) are unknown. The FO-identity in eq. (4.9) and the explicit examples previously discussed show, however, the way to construct successive approximants to $G_{\mathrm{FO}}(X)$. The particular approximants that emerge from the leading non-analytic contributions discussed in the previous subsection are defined by successive power series of N terms, plus a linear combination of the three types of singular functions in eqs. (4.14) and (4.18) i.e.,

$$\begin{aligned} G_{\mathrm{FO}}(X) \approx G_{\mathrm{FO}}^{\left(N;\frac{3}{2};\frac{5}{2},\frac{5'}{2}\right)}(X) = \sum_{n=0}^{N} \mathcal{A}_n \left(\frac{1-X^2}{1+X^2}\right)^n + \frac{\mathcal{B}_{-1,\frac{3}{2}}}{\eta\left(\frac{3}{2}\right)} \mathrm{Li}_{\frac{3}{2}}\left(-\frac{1-X^2}{1+X^2}\right) \\ + \frac{\mathcal{B}_{1,\frac{5}{2}}}{\zeta\left(\frac{5}{2}\right)} \mathrm{Li}_{\frac{5}{2}}\left(\frac{1-X^2}{1+X^2}\right) + \frac{\mathcal{B}'_{1,\frac{5}{2}}}{\zeta'\left(\frac{5}{2}\right)} \mathrm{Li}^{(1,0)}_{\frac{5}{2}}\left(\frac{1-X^2}{1+X^2}\right) , \end{aligned} \tag{4.19}$$

with coefficients

$$\mathcal{A}_n = g_n - g_n^{\mathrm{AS}} , \quad \mathcal{B}_{-1,\frac{3}{2}} , \quad \mathcal{B}_{1,\frac{5}{2}} , \tag{4.20}$$

that are unknown parameters (they will be the free parameters in the fits discussed later); exceptionally the coefficient

$$\mathcal{B}'_{1,\frac{5}{2}} = \frac{3}{16\sqrt{2\pi}} \zeta'\left(\frac{5}{2}\right) \mathrm{s}_{3,1} , \tag{4.21}$$

is known because $\mathrm{s}_{3,1}$ given in eq. (4.5) is fixed by χ_0.[3] The polylog functions in eq. (4.19) have been normalized, for convenience, to their values at $X = 0$ where $\zeta(s)$ denotes the Riemann zeta-function and $\eta(s)$, $\zeta'(s)$ the related functions:

$$\begin{aligned} \eta(s) = \mathrm{Li}_s(-1) = \sum_{n=1}^{\infty} \frac{(-1)^n}{n^s} , \quad \zeta(s) = \mathrm{Li}_s(1) = \sum_{n=1}^{\infty} \frac{1}{n^s} , \\ \zeta'(s) = \mathrm{Li}_s^{(1,0)}(1) = -\sum_{n=1}^{\infty} \frac{\ln n}{n^s} . \end{aligned} \tag{4.22}$$

[3] In fact, all the coefficients $\mathrm{s}_{2n,n}$ for $n \geq 1$ depend only on a_{-3} and χ_0.

JHEP03(2023)248

The parameters in eq. (4.20) are further restricted by the two sum rules:

$$0 = \sum_{n=1}^{N} \mathcal{A}_n + \mathcal{B}_{-1,\frac{3}{2}} + \mathcal{B}_{1,\frac{5}{2}} + \mathcal{B}'_{1,\frac{5}{2}} \,, \tag{4.23}$$

$$0 = \sum_{n=1}^{N} (-1)^n \mathcal{A}_n + \mathcal{B}_{-1,\frac{3}{2}} \frac{\zeta\left(\frac{3}{2}\right)}{\eta\left(\frac{3}{2}\right)} + \mathcal{B}_{1,\frac{5}{2}} \frac{\eta\left(\frac{5}{2}\right)}{\zeta\left(\frac{5}{2}\right)} + \mathcal{B}'_{1,\frac{5}{2}} \frac{\eta'\left(\frac{5}{2}\right)}{\zeta'\left(\frac{5}{2}\right)} \,, \tag{4.24}$$

$$\text{where} \quad \eta'(s) = \mathrm{Li}_s^{(1,0)}(-1) = -\sum_{n=1}^{\infty} \frac{\ln n}{n^s} (-1)^n \,, \tag{4.25}$$

which guarantee that the asymptotic behaviours

$$\lim_{X\to 0} G_{\mathrm{FO}}(X) = 0 \quad \text{and} \quad \lim_{X\to\infty} G_{\mathrm{FO}}(X) = 0 \tag{4.26}$$

are satisfied.

The reason why the polynomials in eq. (4.19) are of finite degree N is due to the fact that only the contribution of the leading non-analytic terms has been taken into account in the construction of the approximants. One expects, therefore, that beyond a certain critical N value depending also on the input number of LQCD $G(x_0)$ values, the approximants will cease to improve. It is possible, however, to correct this by adding successive extra contributions associated to the subleading non-analytic terms, but it requires the introduction of extra $\mathcal{A}_n$ parameters as well as further singular functions modulated by extra unknown $\mathcal{B}$-like parameters and, furthermore, a more refined and/or extended set of $G(x_0)$ input values. In this work we shall, therefore, only consider the leading set of approximants defined in eq. (4.19) which, as we shall see, already produce significantly accurate results.

The values of the unknown parameters in eq. (4.20), restricted to satisfy the two sum rules above, can then be obtained from a linear fit of the successive $G_{\mathrm{FO}}^{\left(N;\frac{3}{2};\frac{5}{2},\frac{5'}{2}\right)}(X)$ approximants in eq. (4.19) to the data input provided by LQCD evaluations of $G(x_0)$ in a given optimal x_0-region. It is always possible to have a solution for the unknown parameters provided that: with $\boldsymbol{\mathcal{A}} = \{\mathcal{A}_0, \ldots, \mathcal{A}_N\}$ and $\boldsymbol{\mathcal{G}} = \{\mathcal{G}(x_0), \ldots, \mathcal{G}(x_N)\}$ where

$$\mathcal{G}(\varphi_i) = G_{\mathrm{FO}}(\varphi_i) - \frac{\mathcal{B}'_{1,\frac{5}{2}} \zeta'\left(\frac{5}{2}\right)}{2\zeta^2\left(\frac{5}{2}\right)} \left[[c_1(0) - c_1(1)]\, \mathrm{Li}_{\frac{3}{2}}(-\varphi_i) + [c_2(0) - c_2(1)]\, \mathrm{Li}_{\frac{5}{2}}(\varphi_i) \right.$$
$$\left. + 2 \frac{\zeta\left(\frac{5}{2}\right)}{\zeta'\left(\frac{5}{2}\right)} \mathrm{Li}_{\frac{5}{2}}^{(1,0)}(\varphi_i) \right] \,, \tag{4.27}$$

the matrix $\mathbb{M}$ such that $\mathbb{M} \cdot \boldsymbol{\mathcal{A}} = \boldsymbol{\mathcal{G}}$ is invertible. This implies the condition

$$\det \mathbb{M} \equiv \det \left[\varphi_i^j + c_1(j)\, \mathrm{Li}_{\frac{3}{2}}(-\varphi_i) + c_2(j)\, \mathrm{Li}_{\frac{5}{2}}(\varphi_i) \right]_{i,j} \neq 0 \,,$$

JHEP03(2023)248

with

$$c_1(j) = \frac{4\sqrt{2}(-1)^j - 2 + 4\sqrt{2}}{\left(\sqrt{2}-6\right)\zeta\left(\frac{3}{2}\right)} \quad \text{and} \quad c_2(j) = \frac{4\left(\left(\sqrt{2}-1\right)(-1)^j + \sqrt{2}\right)}{\left(\sqrt{2}-6\right)\zeta\left(\frac{5}{2}\right)}\,, \tag{4.28}$$

to be satisfied.

We illustrate in the next section how to implement this procedure with a phenomenological model that simulates the hadronic spectral function.

5 Illustration with a phenomenological model

The spectral function of the model in question is inspired from lowest order χPT, ρ-vector meson dominance, and asymptotic freedom:

$$\frac{1}{\pi}\,\mathrm{Im}\,\Pi^{\mathrm{HVP}}_{\mathrm{model}}(t) = \frac{\alpha}{\pi}\left(1-\frac{4m_\pi^2}{t}\right)^{3/2}\left\{\frac{1}{12}|F(t)|^2 + \sum_{\mathrm{quarks}} e_q^2\;\;\Theta(t,t_c,\Delta)\right\}\theta(t-4m_\pi^2)\,. \tag{5.1}$$

It consists of a Breit-Wigner-like modulous squared form factor[4]

$$|F(t)|^2 = \frac{M_\rho^4}{(M_\rho^2-t)^2 + M_\rho^2\,\Gamma(t)^2}\,, \tag{5.2}$$

with an energy dependent width

$$\Gamma(t) = \frac{M_\rho t}{96\pi f_\pi^2}\left[\left(1-\frac{4m_\pi^2}{t}\right)^{3/2}\theta(t-4m_\pi^2) + \frac{1}{2}\left(1-\frac{4M_k^2}{t}\right)^{3/2}\theta(t-4M_k^2)\right]\,; \tag{5.3}$$

plus a function

$$\Theta(t,t_c,\Delta) = \frac{\frac{2}{\pi}\arctan\left(\frac{t-t_c}{\Delta}\right) - \frac{2}{\pi}\arctan\left(\frac{t_0-t_c}{\Delta}\right)}{1-\frac{2}{\pi}\arctan\left(\frac{t_0-t_c}{\Delta}\right)}\,, \tag{5.4}$$

that has two arbitrary parameters t_c and Δ and smoothly matches the low energy behaviour to the asymptotic pQCD continuum. The shape of this spectral function, using the physical central values for m_π, M_k, M_ρ, $f_\pi = 93.3\,\mathrm{MeV}$, and the choice: $t_c = 1\,\mathrm{GeV}^2$ and $\Delta = 0.5\,\mathrm{GeV}^2$, with $\sum_{\mathrm{quarks}} e_q^2 = \frac{5}{3}$, is shown in figure 4.

The shape of the TMR function of the model

$$x_0^3\;G_{\mathrm{model}}(x_0) = x_0^3\int_{\sqrt{t_0}}^{\infty} d\omega\;e^{-\omega x_0}\;\omega^2\,\frac{1}{\pi}\,\mathrm{Im}\,\Pi^{\mathrm{HVP}}_{\mathrm{model}}(\omega^2)\,, \tag{5.5}$$

is shown in figure 6. The same function plotted in terms of the variable φ in eq. (4.8) is shown in figure 5. Its contribution to the muon anomaly, using only the center values of the parameters given above, is

$$\left(a_\mu^{\mathrm{HVP}}\right)_{\mathrm{model}} = 6\;992\times 10^{-11}\,. \tag{5.6}$$

[4]This is a simplified version of phenomenological spectral functions discussed in the literature, e.g. in refs. [40, 41] and references therein.

JHEP03(2023)248

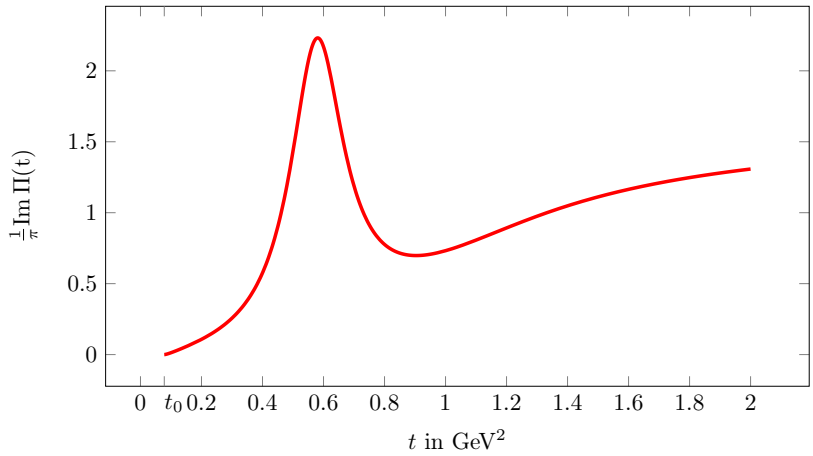

Figure 4. The model spectral function in eq. (5.1) for $t_c = 1\,\mathrm{GeV}^2$ and $\Delta = 0.5\,\mathrm{GeV}^2$ in $\frac{\alpha}{\pi}$-units.

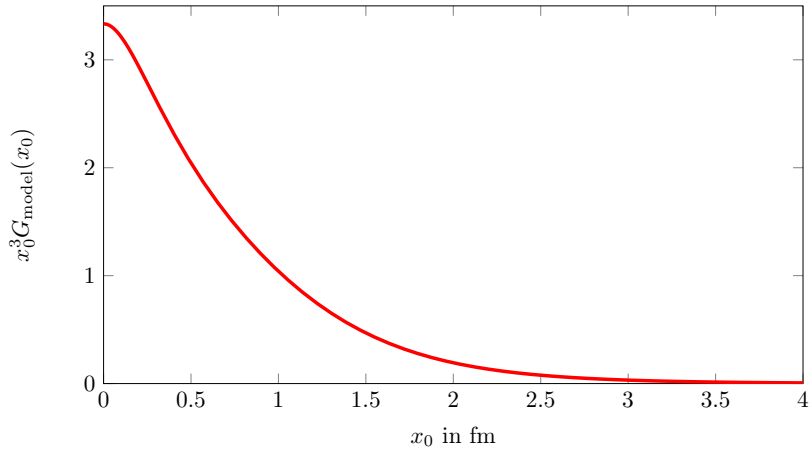

Figure 5. The model TMR function $x_0^3\, G_{\mathrm{model}}(x_0)$ in eq. (5.5) in $\frac{\alpha}{\pi}$ units.

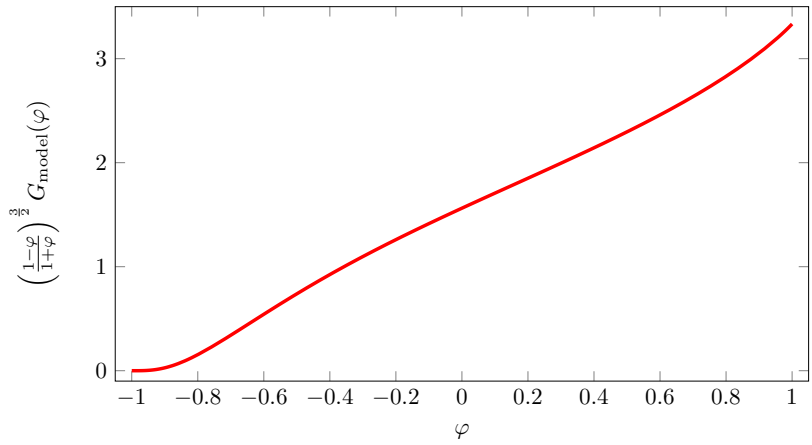

Figure 6. The model TMR function $x_0^3\, G_{\mathrm{model}}(x_0)$ as a function of the φ variable in $\frac{\alpha}{\pi}$ units.

JHEP03(2023)248

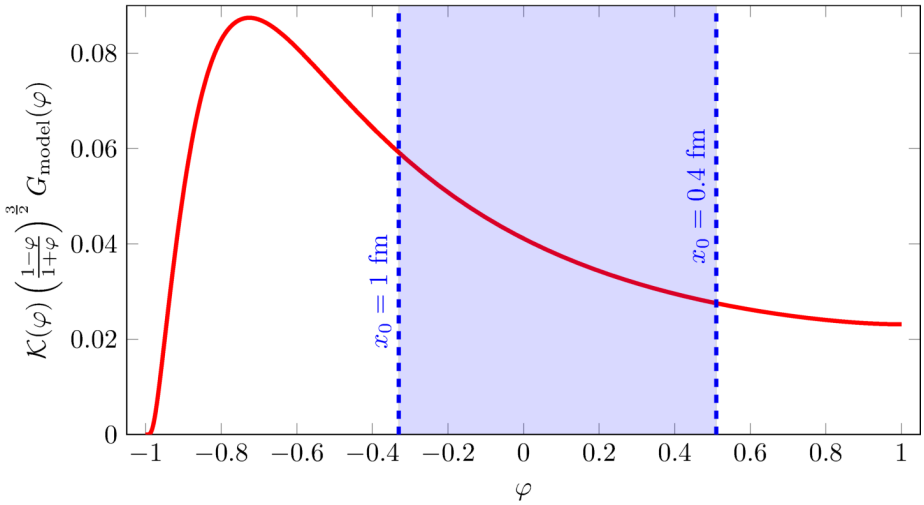

Figure 7. Shape of the integrand of $\left(a_\mu^{\rm HVP}\right)_{\rm model}$ in $\frac{\alpha}{\pi}\frac{m_\mu^2}{t_0}$ units as a function of φ.

We also show the shape of the integrand of $\left(a_\mu^{\rm HVP}\right)_{\rm model}$ as a function of the φ variable in figure 7. Notice that in this representation, the intermediate region $0.4\,{\rm fm} \leq x_0 \leq 1.0\,{\rm fm}$ favoured by the LQCD evaluations and shown in blue, corresponds to the interval $0.51 \geq \varphi \geq -0.33$. One can see that, in spite of the exponential decrease of $G(x_0)$ at large x_0 (small φ), the contribution to $\left(a_\mu^{\rm HVP}\right)_{\rm model}$ from the long-distance region $-1.0 \geq \varphi \geq -0.33$ is highly weighted; a fact that demands a good reconstruction of $G(x_0)$ in the low-energy region (large-x_0) in order to have an accurate evaluation of $\left(a_\mu^{\rm HVP}\right)_{\rm model}$. This we expect to be a generic feature in QCD as well.

The function

$$G_{\rm FO}^{\rm model}(x_0) \equiv \frac{G_{\rm model}(x_0)}{G^*(x_0)} - 1\,, \tag{5.7}$$

with the two parameters of the $G^*(x_0)$ function adjusted to the asymptotic behaviours of the model, i.e. $a_{-3} = \frac{10}{3}$ and $\chi_0 = 0.31$, is plotted in figure 8 in black for a finite x_0 interval. This shape is what the successive FO-approximants in eq. (4.19) are expected to reproduce, all the way from $x_0 = 0$ to $x_0 = \infty$ (i.e. from $\varphi = 1$ to $\varphi = -1$). The red dots in the figure are the points used in the fit described in section 5.1. More compact plots of the $G_{\rm FO}^{\rm model}$ function in terms of the φ-variable are shown in figure 9 for $-1 \leq \varphi \leq -0.5$ and in figure 10 for $-0.5 \leq \varphi \leq -1$.

5.1 Fits to the model data using FO-approximants

The input we use as an example are the values of the function $G_{\rm FO}^{\rm model}(x_0)$ at twelve points, equally spaced with no errors, in the intermediate region[5]

$$0.4\,{\rm fm} \leq x_0 \leq 1.0\,{\rm fm}\,. \tag{5.8}$$

The corresponding data points are shown as red dots in figure 8 and figure 10. We then make linear fits of the successive FO-approximants defined in eqs. (4.19), (4.23) and (4.24) to

[5]This is the x_0-region where at present LQCD simulations are most precise [5, 8–10].

JHEP03(2023)248

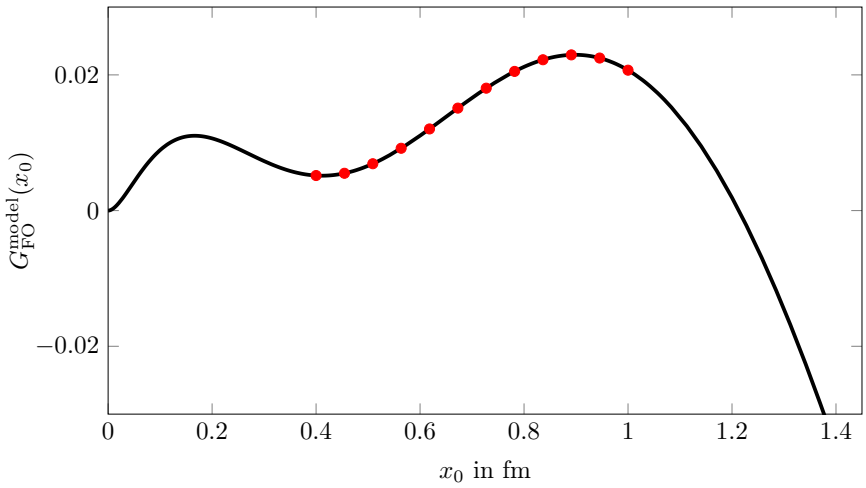

Figure 8. Shape of the $G_{\rm FO}^{\rm model}(x_0)$ function in eq. (5.7) in the interval $0 \leq x_0 \leq 1.4\,\text{fm}$.

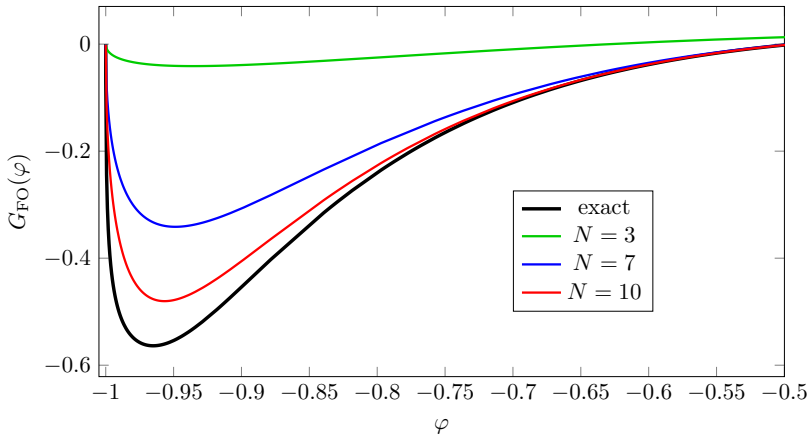

Figure 9. Shape of the Approximants $G_{\rm FO}^{\left(N;\frac{3}{2};\frac{5}{2},\frac{5'}{2}\right)}(\varphi)$ for $N = 3$ (green), $N = 7$ (blue) and $N = 10$ (red). The model function $G_{\rm FO}^{\rm model}(\varphi)$ which the approximants are expected to approach is in black.

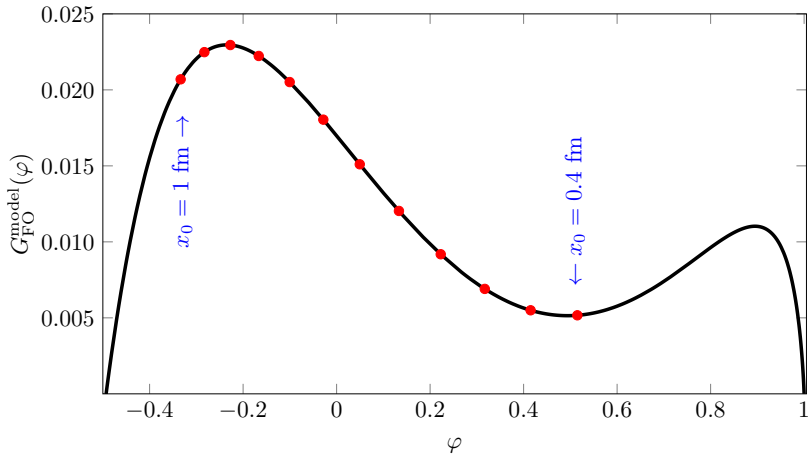

Figure 10. Shape of the $G_{\rm FO}^{\rm model}(\varphi)$ function in the interval $-0.5 \leq \varphi \leq 1$.

JHEP03(2023)248

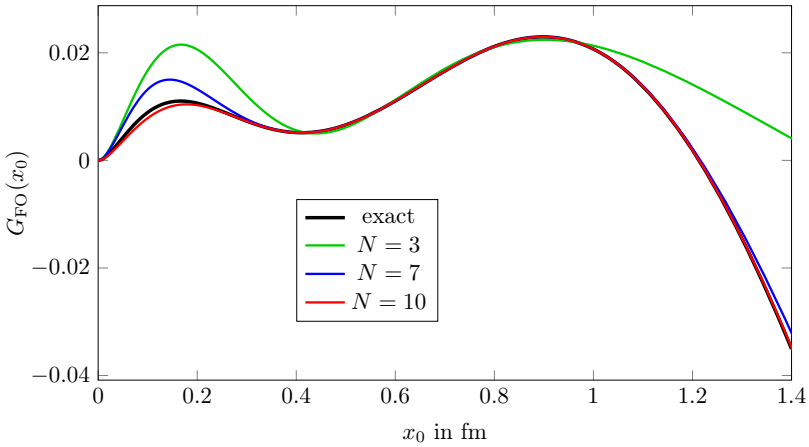

Figure 11. Shape of the Approximants $G_{\rm FO}^{\left(N;\frac{3}{2},\frac{5}{2},\frac{5'}{2}\right)}(x_0)$ in eq. (4.19) for $N = 3$ (green), $N = 7$ (blue) and $N = 10$ (red). The model function $G_{\rm FO}^{\rm model}(x_0)$ which the approximants are expected to approach is in black.

the $G_{\rm FO}^{\rm model}(x_0)$ function in eq. (5.7), and this way obtain the values of the free parameters of each approximant that fix the reconstruction of the $G_{\rm FO}^{\rm model}(x_0)$ function in the full $0 \leq x_0 \leq \infty$ range. The corresponding reconstruction of $G(x_0)$ follows then from eq. (5.7).

The quality of the fits is shown in figure 11 for the approximants with $N = 3$ in green, $N = 7$ in blue and $N = 10$ in red. The shape of $G_{\rm FO}^{\rm model}(x_0)$ is shown in black. One can see how the reconstruction in the extended region $0.0\,\text{fm} \leq x_0 \leq 1.5\,\text{fm}$ beyond the one used for the fit, improves as N increases. The blue (N=7) and red (N=10) curves are already quite closed to the $G_{\rm FO}^{\rm model}(x_0)$ black curve.

In order to show the shapes of the approximants in the full $0 \leq X \leq \infty$ it is better to use the representation in terms of the equivalent φ variable, covering the full range $-1 \leq \varphi \leq 1$. This is shown in figure 9 for $-1.0 \leq \varphi \leq -0.5$ and, in a different scale, in figure 12 for $-0.5 \leq \varphi \leq 1.0$.

The contribution of each approximant to the muon anomaly is then given by the integral

$$a_\mu(N) = \int_0^\infty dX\, \mathcal{K}(X)\, X^3\, G^*(X) \left[1 + G_{\rm FO}^{\left(N;\frac{3}{2},\frac{5}{2},\frac{5'}{2}\right)}(X)\right], \tag{5.9}$$

where $\mathcal{K}(X)$ is the kernel defined in eq. (3.8) and $G_{\rm FO}^{\left(N;\frac{3}{2},\frac{5}{2},\frac{5'}{2}\right)}(X)$ the approximant defined in eq. (4.19) with the values of the free parameters fixed by the fit. The results for each N-approximant compared to the exact result in eq. (5.6) are given in table 1. The errors in % are the values of

$$\texttt{Err}(N) = \left|\frac{a_\mu(N) - a_\mu^{\rm model}}{a_\mu(N) + a_\mu^{\rm model}}\right| 2 \times 10^2\,. \tag{5.10}$$

JHEP03(2023)248

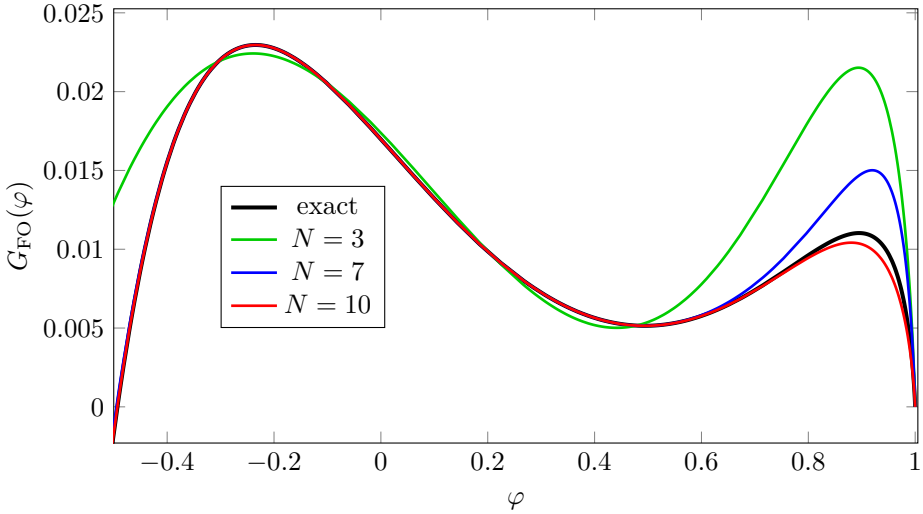

Figure 12. Shape of the Approximants $G_{\rm FO}^{\left(N;\frac{3}{2};\frac{5}{2},\frac{5'}{2}\right)}(\varphi)$ for $N = 3$ (green), $N = 7$ (blue) and $N = 10$ (red) and their matching to the model function $G_{\rm FO}^{\rm model}(\varphi)$ (black). The model function $G_{\rm FO}^{\rm model}(\varphi)$ which the approximants are expected to approach is in black. The red and black curves in this region are already practically identical. Notice the vertical scale in the figure.

N	$a_\mu(N)$ in 10^{-11} units	$\texttt{Err}(N)$ in %
1	7814	11
2	7696	9.6
3	7597	8.3
4	7446	6.3
5	7335	4.8
6	7233	3.4
7	7162	2.4
8	7104	1.6
9	7066	1.0
10	7043	0.7
11	6990	0.04

Table 1. Predicted values of the model anomaly from the approximants defined in eq. (5.9) and the errors in % defined by eq. (5.10) in the third column.

5.2 Errors of the FO-approximants

The results in table 1 show that the approximants reproduce the value of $a_\mu^{\rm model}$ with better and better accuracy as N increases. The best result is obtained for $N = 11$ when the number of free parameters equals the number of input points and the linear fit corresponds then to solving a linear system of N equations with N unknowns. These results are very encouraging, however, in a potential application of the FO-Approximants to LQCD one will have to take into account the errors of the input data as well as an evaluation of the expected error associated to the FO-Approximants. Inclusion of the errors of the LQCD

JHEP03(2023)248

data is beyond the scope of this paper,[6] but two obvious questions which require answers on our part are:

1. *Given a finite number of $G(x_0)$ input values from LQCD simulations, and given the N results of the successive reconstructions of the full $G(x_0)$ function using FO-approximants, what is the optimal value of $a_\mu^{\rm HVP}$ and what error should be assigned to it?*
2. *Can one give a systematic error to the method of FO-Approximants?*

An answer to the first question follows from the observation in table 1 that

$$a_\mu(N+1) < a_\mu(N) \quad \text{for all} \quad N = 1 \text{ to } 11\,. \tag{5.11}$$

- If this decreasing pattern persists in the case of an application to LQCD, the value $a_\mu(N^*)$ from the FO-approximant with $N = N^*$ i.e. the total number of input values, is clearly the optimal choice. In this case it seems natural to assign as the error attributed to each $a_\mu(N)$ approximant the difference $|a_\mu(N) - a_\mu(N^*)|$. Provided that N is sufficiently large, the optimal value is then:

$$a_\mu^{\rm optimal} = a_\mu(N^*) \pm |a_\mu(N^*-1) - a_\mu(N^*)|\,. \tag{5.12}$$

- If the pattern of the $a_\mu(N)$ estimates, as N increases, has a minimum or a maximum at a given N^*-value, then the optimal choice is the same as before with N^* at the value of the extrema.
- If the pattern of the $a_\mu(N)$ approximants oscillates as N increases then the most natural optimal choice is the one at the N^* closest to the mean value of all the approximants.

In order to get an estimate of the *systematic error* of the method of FO-approximants when applied to a finite set of input values of $G(x_0)$, let us consider the extreme case where $G(x_0) = G^*(x_0)$. The corresponding function $G_{\rm FO}(x_0)$ is then, by definition, trivially zero. However, because of the *systematic errors* of the FO-approximants, one expects deviations from zero from the results of the approximants in the x_0 regions outside the one used as an input in the fit, and this is what one observes. Since in this case we know exactly the value of the muon anomaly (the one given by the chosen $G^*(x_0)$), we can define as a *systematic error* of each approximant the one which follows from applying the definition in eq. (5.10) to this case where $a_\mu(\text{model}) = a_\mu^*$. We show in table 2 this resulting systematic error for each FO-approximant.

We have also analyzed the results of the FO-approximants in the following alternative situations:

- With only six input points, equally spaced, in the interval 0.4 fm to 1 fm one gets

$$a_\mu(5) = 7327 \times 10^{-11} \tag{5.13}$$

  which reproduces the model value at the level of 5%. The number of input points is however too small to give a significant systematic error in this case.

[6] This is something to be discussed with each LQCD collaboration.

JHEP03(2023)248

N	`ErrorSyst`(N) in %
1	1.00711
2	0.20572
3	0.16359
4	0.04585
5	0.05261
6	0.01495
7	0.02230
8	0.00484
9	0.01052
10	0.00070
11	0.00524

Table 2. Systematic error in % attributed to each FO-approximant defined in eq. (5.9).

- With an input of 10 points, equally spaced, but in the larger interval 0.3 fm to 1.2 fm as compared to the 0.4 fm to 1.0 fm interval used above, one gets

$$a_\mu(11) = 7003 \times 10^{-11} \tag{5.14}$$

which reproduces the model value to 0.15% with a systematic error of 0.2%:

$$a_\mu^{\text{optimal}} = (7003 \pm 15) \times 10^{-11} \tag{5.15}$$

and indicates that using the same number of input points in a larger interval improves the result of the FO-approximants.

6 Conclusion and outlook

We have shown how the FO-theorem can be used to reconstruct the TMR function $G(x_0)$ in its full $0 \leq x_0 \leq \infty$ domain, when one only uses as an input its values in a restricted x_0-domain where LQCD evaluations are most precise. We have explicitly derived the functional form of the reconstruction approximants that emerge from the properties of the FO-theorem. These FO-approximants depend linearly on a set of N parameters that are related to the successive terms of the short-distance and long-distance expansions of the $G(x_0)$ function in QCD. The specific values of these QCD parameters are unknown, but they can be fixed from a fit of the FO-approximants to the LQCD evaluation of $G(x_0)$ in an optimal region. In section 5 we have illustrated the procedure to follow in an eventual application to LQCD, with the simulation of a phenomenological model which captures the leading short and long distance behaviours of HVP in QCD. The application of FO-approximants in this case shows how the reconstruction of the model TMR function $G_{\text{model}}(x_0)$ improves as the number N of terms in the FO-approximant increases: using an input of twelve points, equally spaced with no errors, in the intermediate region $0.4\,\text{fm} \leq x_0 \leq 1.0\,\text{fm}$, we find that the best FO-approximant reproduces the value: $\left(a_\mu^{\text{HVP}}\right)_{\text{model}} = 6\ 992 \times 10^{-11}$ to an

JHEP03(2023)248

accuracy of 0.6%. We find these results encouraging and worth considering for applications to the reconstruction of the $G(x_0)$ function in LQCD and the corresponding evaluations of $a_\mu^{\rm HVP}$ from first principles.

Concerning the comparison of LQCD results with the data driven determinations in eqs. (1.5) we suggest considering the case where the so called *skeleton function* introduced in sections 3.2 and 4 is chosen to be the one resulting from the data-driven determination of HVP. It is well known that the shape of this function is at present in disagreement with LQCD determinations in intermediate x_0-windows (see e.g. refs. [8, 10, 12]). The corresponding $G_{\rm FO}(x_0)$ function defined in section 4 will, therefore, be different from zero in these windows. The application of the FO-approximants in this case provides a way to evaluate how this difference propagates outside the region of x_0 used as an input. Comparing the optimal $a_\mu^{\rm HVP}(N^*)$ value obtained from the FO-approximants to the data driven results in eqs. (1.5) would give an evaluation of the total discrepancy.

Acknowledgments

We thank Jérôme Charles for his participation at the early stages of this work. We are grateful to Jérôme Charles, Marc Knecht and Harvey B. Meyer for a careful reading of the manuscript and their comments.

A Mathematical details of the FO-theorem

In full generality, the short-distance expansion in eq. (4.11) and the long-distance expansion in eq. (4.16) are given by the sums:

$$G_{\rm FO}\left(X=\frac{\sqrt{1-\varphi}}{\sqrt{1+\varphi}}\right)\underset{\varphi\to 1}{\sim}\sum_{n\geqslant 2}\sum_{\ell\geqslant 0}\tilde{\mathrm{s}}_{\frac{n}{2},\ell}(1-\varphi)^{\frac{n+\ell}{2}}\ln^\ell(1-\varphi) \tag{A.1}$$

$$G_{\rm FO}\left(X=\frac{\sqrt{1-\varphi}}{\sqrt{1+\varphi}}\right)\underset{\varphi\to -1}{\sim}\sum_{n\geqslant 1}\tilde{\mathrm{l}}_{\frac{n}{2}}(1+\varphi)^{\frac{n}{2}}\,, \tag{A.2}$$

where the $\tilde{\mathrm{s}}_{\frac{n}{2},\ell}$ and $\tilde{\mathrm{l}}_{\frac{n}{2}}$ coefficients are linear combinations of the $\mathrm{s}_{\frac{n}{2},\ell}$ and $\mathrm{l}_{\frac{n}{2}}$ coefficients in eqs. (4.2). The type of singular terms that appear in these expansions are:

For k and ℓ integer numbers,

$$(1-\varphi)^k\ln^\ell(1-\varphi)\quad\text{for}\quad\varphi\to 1\,, \tag{A.3}$$

$$(1-\varphi)^{\frac{2k+1}{2}}\quad\text{and}\quad(1-\varphi)^{\frac{2k+1}{2}}\ln^\ell(1-\varphi)\quad\text{for}\quad\varphi\to 1\,; \tag{A.4}$$

and

$$(1+\varphi)^{\frac{2k+1}{2}}\quad\text{for}\quad\varphi\to -1\,. \tag{A.5}$$

The FO-theorem gives the results for the large n behaviour of the coefficients $g_n^{\rm AS}$ in the φ^n power series in eq. (4.9), associated to these four types of singular terms. They can be found in the appendix II of ref. [21] and are given below.

JHEP03(2023)248

- **For $\ell = 1$ in eq. (A.3):**

$$(1-\varphi)^k \ln(1-\varphi) \longmapsto -\frac{(-1)^k \Gamma(k+1)}{n^{k+1}} \sum_{j=0}^{\infty} \left\{ {k+j \atop m} \right\} \frac{1}{n^j}\,, \tag{A.6}$$

where the symbol $\left\{ {\cdot \atop \cdot} \right\}$ denotes Stirling numbers of the second kind.

- **For the first term in eq. (A.4).**
The result can be directly obtained from the evaluation of the φ^n coefficient of its Taylor series at $\varphi \to 0$, and then its behaviour as $n \to \infty$:

$$[\varphi^n] \quad (1-\varphi)^{\frac{2k+1}{2}} = \frac{\Gamma\left(-\frac{2k+1}{2}+n\right)}{\Gamma\left(-\frac{2k+1}{2}\right)\Gamma(n+1)} \underset{n\to\infty}{\sim} \frac{1}{n^{1+\frac{2k+1}{2}}} \sum_{j=0}^{\infty} \frac{\mathrm{B}_j^{\left[-\frac{2k+1}{2}\right]}\left(-\frac{2k+1}{2}\right)}{\Gamma\left(-\frac{2k+1}{2}-j\right)\Gamma(1+j)} \frac{1}{n^j}\,, \tag{A.7}$$

where $\mathrm{B}_n^{[a]}(x)$ are the so-called *generalized Bernoulli polynomials* [39] or *Nørlund polynomials* (as encoded in Mathematica $\mathrm{B}_n^{[a]}(x) = \texttt{Norlund}[n,a,x]$). Their first few terms are

$$\mathrm{B}_0^{[\lambda]}(\lambda) = 1\,,\ \mathrm{B}_1^{[\lambda]}(\lambda) = \frac{\lambda}{2}\,,\ \mathrm{B}_2^{[\lambda]}(\lambda) = \frac{1}{12}\lambda(3\lambda-1)\,,\ldots\,. \tag{A.8}$$

In particular, for $k=1$, this is the way that the result in eq. (4.12) follows

$$(1-\varphi)^{\frac{3}{2}} \longmapsto \frac{2}{\sqrt{\pi}} \frac{1}{n^{\frac{5}{2}}} \left[1 + \frac{15}{8}\frac{1}{n} + \frac{385}{128}\frac{1}{n^2} + \cdots\right]. \tag{A.9}$$

- **For the second term in eq. (A.4).**
We use the property that

$$(1-\varphi)^{\frac{2k+1}{2}} \ln^\ell(1-\varphi) = \frac{\partial^\ell}{\partial\varepsilon^\ell}\left[(1-\varphi)^{\frac{2k+1}{2}+\varepsilon}\right]_{\varepsilon=0}\,, \tag{A.10}$$

where from the coefficient of the φ^n term of its Taylor series at $\varphi \to 0$ can be easily calculated

$$[\varphi^n]\,(1-\varphi)^{\frac{2k+1}{2}} \ln^\ell(1-\varphi) = \frac{\partial^\ell}{\partial\varepsilon^\ell}\left[[\varphi^n]\,(1-\varphi)^{\frac{2k+1}{2}+\varepsilon}\right]_{\varepsilon=0} \tag{A.11}$$

$$= \frac{\partial^\ell}{\partial\varepsilon^\ell}\left[\frac{\Gamma\left(-\frac{2k+1}{2}-\varepsilon+n\right)}{\Gamma\left(-\frac{2k+1}{2}-\varepsilon\right)\Gamma(n+1)}\right]_{\varepsilon=0}. \tag{A.12}$$

Only the case $\ell = 1$ is needed in our case with the result

$$[\varphi^n]\,(1-\varphi)^{\frac{2k+1}{2}} \ln(1-\varphi)$$

$$= \frac{\Gamma\left(-\frac{2k+1}{2}+n\right)}{\Gamma\left(-\frac{2k+1}{2}\right)\Gamma(n+1)}\left[\psi\left(-\frac{2k+1}{2}\right) - \psi\left(n-\frac{2k+1}{2}\right)\right] \tag{A.13}$$

$$\underset{n\to\infty}{\sim} \frac{-\ln n + \psi\left(-\frac{2k+1}{2}\right)}{n^{1+\frac{2k+1}{2}}} \sum_{j=0}^{\infty} \frac{\mathrm{B}_j^{\left[-\frac{2k+1}{2}\right]}\left(-\frac{2k+1}{2}\right)}{\Gamma\left(-\frac{2k+1}{2}-j\right)\Gamma(1+j)} \frac{1}{n^j} - \frac{1}{n^{1+\frac{2k+1}{2}}} \sum_{j=0}^{\infty} \frac{\mathsf{b}_j\left(-\frac{2k+1}{2}\right)}{n^j}\,, \tag{A.14}$$

JHEP03(2023)248

where the $\mathtt{b}_j(\lambda)$ are the polynomials

$$\mathtt{b}_j(\lambda) = \frac{\delta_{j,0}}{\Gamma(\lambda)} + \sum_{m=1}^{j} \frac{\mathrm{B}^{[\lambda]}_{j-m}(\lambda)}{\Gamma(\lambda-j+m)\,\Gamma(1+j-m)} \frac{(-1)^m\,\mathrm{B}^{[1]}_m(\lambda)}{m}\,, \tag{A.15}$$

and where we have also used the fact that

$$\psi(n-\lambda) \underset{n\to\infty}{\sim} \ln n + \sum_{p=1}^{\infty} \frac{(-1)^p\,\mathrm{B}^{[1]}_p(\lambda)}{p} \frac{1}{n^p}\,. \tag{A.16}$$

The result in eq. (4.13) is the one which corresponds to the particular case where $\ell = 1$ and $k = 1$

$$\begin{aligned}&(1-\varphi)^{\frac{3}{2}} \ln(1-\varphi) \longmapsto \\ &\quad \frac{2}{\sqrt{\pi}} \frac{1}{n^{\frac{5}{2}}} \left\{ \frac{8}{3} - \gamma_E - \ln 4 - \ln n + \frac{15}{8} \left[\frac{56}{15} - \gamma_E - \ln 4 - \ln n \right] \frac{1}{n} + \cdots \right\}.\end{aligned} \tag{A.17}$$

A general expression for any ℓ can be easily obtained from the results above before using successive derivatives in ε.

- **For the terms in eq. (A.5).**
  The result can be directly obtained from the evaluation of the φ^n coefficient of its Taylor series at $\varphi \to 0$, and then its behaviour as $n \to \infty$:

$$[\varphi^n] \quad (1+\varphi)^{\frac{2k+1}{2}} \quad = \quad (-1)^n \frac{\Gamma\left(-\frac{2k+1}{2}+n\right)}{\Gamma\left(-\frac{2k+1}{2}\right)\Gamma(n+1)} \tag{A.18}$$

$$\underset{n\to\infty}{\sim} \frac{(-1)^n}{n^{1+\frac{2k+1}{2}}} \sum_{j=0}^{\infty} \frac{\mathrm{B}_j^{\left[-\frac{2k+1}{2}\right]}\left(-\frac{2k+1}{2}\right)}{\Gamma\left(-\frac{2k+1}{2}-j\right)\Gamma(1+j)} \frac{1}{n^j}\,. \tag{A.19}$$

The final expression for the g_n^{AS} coefficients follows from the sum of the results given in the three items discussed above i.e.,

$$g_n \underset{n\to\infty}{\sim} g_n^{\mathrm{AS}} = \frac{\mathcal{B}_{-1,\frac{3}{2}}}{\eta\left(\frac{3}{2}\right)} \frac{(-1)^n}{n^{\frac{3}{2}}} + \frac{\mathcal{B}_{1,\frac{5}{2}}}{\zeta\left(\frac{5}{2}\right)} \frac{1}{n^{\frac{5}{2}}} - \frac{\mathcal{B}'_{1,\frac{5}{2}}}{\zeta'\left(\frac{5}{2}\right)} \frac{\ln n}{n^{\frac{5}{2}}}, \tag{A.20}$$

where the coefficient $\mathcal{B}_{-1,\frac{3}{2}}$ is proportional to l_1 and the coefficients $\mathcal{B}_{1,\frac{5}{2}}$ and $\mathcal{B}'_{\frac{5}{2}}$ are a linear combination of the $\mathrm{s}_{n,\ell}$ coefficients.

Open Access. This article is distributed under the terms of the Creative Commons Attribution License (CC-BY 4.0), which permits any use, distribution and reproduction in any medium, provided the original author(s) and source are credited. SCOAP^3 supports the goals of the International Year of Basic Sciences for Sustainable Development.

JHEP03(2023)248

References

[1] Muon $g-2$ collaboration, *Final Report of the Muon E821 Anomalous Magnetic Moment Measurement at BNL*, *Phys. Rev. D* **73** (2006) 072003 [hep-ex/0602035] [INSPIRE].

[2] Muon $g-2$ collaboration, *Measurement of the Positive Muon Anomalous Magnetic Moment to* 0.46 *ppm*, *Phys. Rev. Lett.* **126** (2021) 141801 [arXiv:2104.03281] [INSPIRE].

[3] Muon g-2 collaboration, *Measurement of the anomalous precession frequency of the muon in the Fermilab Muon $g-2$ Experiment*, *Phys. Rev. D* **103** (2021) 072002 [arXiv:2104.03247] [INSPIRE].

[4] T. Aoyama et al., *The anomalous magnetic moment of the muon in the Standard Model*, *Phys. Rept.* **887** (2020) 1 [arXiv:2006.04822] [INSPIRE].

[5] S. Borsanyi et al., *Leading hadronic contribution to the muon magnetic moment from lattice QCD*, *Nature* **593** (2021) 51 [arXiv:2002.12347] [INSPIRE].

[6] M. Davier, A. Hoecker, B. Malaescu and Z. Zhang, *A new evaluation of the hadronic vacuum polarisation contributions to the muon anomalous magnetic moment and to $\alpha(m_Z^2)$*, *Eur. Phys. J. C* **80** (2020) 241 [*Erratum ibid.* **80** (2020) 410] [arXiv:1908.00921] [INSPIRE].

[7] A. Keshavarzi, D. Nomura and T. Teubner, *$g-2$ of charged leptons, $\alpha(M_Z^2)$, and the hyperfine splitting of muonium*, *Phys. Rev. D* **101** (2020) 014029 [arXiv:1911.00367] [INSPIRE].

[8] M. Cè et al., *Window observable for the hadronic vacuum polarization contribution to the muon $g-2$ from lattice QCD*, *Phys. Rev. D* **106** (2022) 114502 [arXiv:2206.06582] [INSPIRE].

[9] C. Alexandrou et al., *Lattice calculation of the short and intermediate time-distance hadronic vacuum polarization contributions to the muon magnetic moment using twisted-mass fermions*, arXiv:2206.15084v2 [INSPIRE].

[10] Fermilab Lattice, HPQCD and MILC collaborations, *Windows on the hadronic vacuum polarization contribution to the muon anomalous magnetic moment*, *Phys. Rev. D* **106** (2022) 074509 [arXiv:2207.04765v1] [INSPIRE].

[11] T. Blum et al., *An update of Euclidean windows of the hadronic vacuum polarization*, arXiv:2301.08696v1 [INSPIRE].

[12] RBC and UKQCD collaborations, *Calculation of the hadronic vacuum polarization contribution to the muon anomalous magnetic moment*, *Phys. Rev. Lett.* **121** (2018) 022003 [arXiv:1801.07224] [INSPIRE].

[13] G. Colangelo et al., *Data-driven evaluations of Euclidean windows to scrutinize hadronic vacuum polarization*, *Phys. Lett. B* **833** (2022) 137313 [arXiv:2205.12963] [INSPIRE].

[14] M. Abe et al., *A New Approach for Measuring the Muon Anomalous Magnetic Moment and Electric Dipole Moment*, *Prog. Theor. Exp. Phys.* **2019** (2019) 053C02 [arXiv:1901.03047] [INSPIRE].

[15] C.M. Carloni Calame, M. Passera, L. Trentadue and G. Venanzoni, *A new approach to evaluate the leading hadronic corrections to the muon $g-2$*, *Phys. Lett. B* **746** (2015) 325 [arXiv:1504.02228] [INSPIRE].

[16] G. Abbiendi et al., *Measuring the leading hadronic contribution to the muon $g-2$ via μe scattering*, *Eur. Phys. J. C* **77** (2017) 139 [arXiv:1609.08987] [INSPIRE].

JHEP03(2023)248

[17] G. Abbiendi, *Letter of Intent: the MUonE project*, CERN-SPSC-2019-026 (2019) [SPSC-I-252].

[18] R.N. Nasheeha, S. Thirukkanesh and F.C. Ragel, *Anisotropic generalization of isotropic models via hypergeometric equation*, *Eur. Phys. J. C* **80** (2020) 6 [INSPIRE].

[19] P. Flajolet and A. Odlyzko, *Singularity Analysis of Generating Functions*, *SIAM J. Discrete Math.* **3** (1990) 216.

[20] P. Flajolet and R. Sedgewick, *Analytic Combinatorics*, Cambridge University Press (2009).

[21] D. Greynat and E. de Rafael, *Hadronic vacuum polarization and the MUonE proposal*, *JHEP* **05** (2022) 084 [arXiv:2202.10810] [INSPIRE].

[22] D. Greynat and S. Peris, *Resummation of Threshold, Low- and High-Energy Expansions for Heavy-Quark Correlators*, *Phys. Rev. D* **82** (2010) 034030 [*Erratum ibid.* **82** (2010) 119907] [arXiv:1006.0643] [INSPIRE].

[23] D. Greynat, P. Masjuan and S. Peris, *Analytic Reconstruction of heavy-quark two-point functions at* $\mathcal{O}(\alpha_s^3)$, *Phys. Rev. D* **85** (2012) 054008 [arXiv:1104.3425] [INSPIRE].

[24] D. Greynat and P. Masjuan, *A new determination of the charm mass from the non-analytic reconstruction of the heavy quark correlator*, *PoS* **Confinement X** (2012) 162 [arXiv:1302.0722] [INSPIRE].

[25] C. Bouchiat and L. Michel, *La résonance dans la diffusion méson* π*-méson* π *et le moment magnétique anormal du méson* μ, *J. Phys. Radium* **22** (1961) 121 [INSPIRE].

[26] S.J. Brodsky and E. de Rafael, *Suggested boson-lepton pair couplings and the anomalous magnetic moment of the muon*, *Phys. Rev.* **168** (1968) 1620 [INSPIRE].

[27] M. Gourdin and E. de Rafael, *Hadronic contributions to the muon g-factor*, *Nucl. Phys. B* **10** (1969) 667 [INSPIRE].

[28] G.J. Gounaris and J.J. Sakurai, *Finite width corrections to the vector meson dominance prediction for* $\rho \to e^+e^-$, *Phys. Rev. Lett.* **21** (1968) 244 [INSPIRE].

[29] D. Bernecker and H.B. Meyer, *Vector Correlators in Lattice QCD: Methods and applications*, *Eur. Phys. J. A* **47** (2011) 148 [arXiv:1107.4388] [INSPIRE].

[30] J. Charles, E. de Rafael and D. Greynat, *Mellin-Barnes approach to hadronic vacuum polarization and* $g_\mu - 2$, *Phys. Rev. D* **97** (2018) 076014 [arXiv:1712.02202] [INSPIRE].

[31] B.E. Lautrup, A. Peterman and E. de Rafael, *Recent developments in the comparison between theory and experiments in quantum electrodynamics*, *Phys. Rept.* **3** (1972) 193 [INSPIRE].

[32] E. de Rafael, *Hadronic contributions to the muon* $g-2$ *and low-energy QCD*, *Phys. Lett. B* **322** (1994) 239 [hep-ph/9311316] [INSPIRE].

[33] T. Blum, *Lattice calculation of the lowest-order hadronic contribution to the muon anomalous magnetic moment*, *Nucl. Phys. B Proc. Suppl.* **140** (2005) 311 [hep-lat/0411002] [INSPIRE].

[34] P. Flajolet, X. Gourdon and P. Dumas, *Mellin transforms and asymptotics: Harmonic sums*, *Theor. Comput. Sci.* **144** (1995) 3.

[35] F.W.J. Olver, *Asymptotics and Special Functions*, 2nd revised edition, A.K. Peters, Ltd., Wellesley, MA, U.S.A. (1997) [ISBN: 1–56881–069–5].

[36] J. Gasser and H. Leutwyler, *Low-Energy Expansion of Meson Form-Factors*, *Nucl. Phys. B* **250** (1985) 517 [INSPIRE].

JHEP03(2023)248

[37] NA7 collaboration, *A Measurement of the Space-Like Pion Electromagnetic Form-Factor*, *Nucl. Phys. B* **277** (1986) 168 [INSPIRE].

[38] Y. Aoki et al., *FLAG Review 2021*, *Eur. Phys. J. C* **82** (2022) 869 [arXiv:2111.09849] [INSPIRE].

[39] F.W.J. Olver et al. eds., *NIST Digital Library of Mathematical Functions*, release 1.1.9 (2023) and online at http://dlmf.nist.gov/.

[40] A. Pich and J. Portoles, *The Vector form-factor of the pion from unitarity and analyticity: A Model independent approach*, *Phys. Rev. D* **63** (2001) 093005 [hep-ph/0101194] [INSPIRE].

[41] G. Colangelo et al., *Chiral extrapolation of hadronic vacuum polarization*, *Phys. Lett. B* **825** (2022) 136852 [arXiv:2110.05493] [INSPIRE].

JHEP03(2023)248